Article

TRANSPARENT PROCESS OPEN ACCESS

EMBO reports

Whole-genome analysis of TET dioxygenase function in regulatory T cells

Xiaojing Yue[1,†], Daniela Samaniego-Castruita[1,2,†], Edahí González-Avalos[1,3], Xiang Li[1,4], Benjamin G Barwick[5,*] & Anjana Rao[1,4,6,**]

Abstract

TET methylcytosine dioxygenases are essential for the stability and function of regulatory T cells (Treg cells), which maintain immune homeostasis and self-tolerance and express the lineage-determining transcription factor Foxp3. Here, we use whole-genome analyses to show that the transcriptional program and epigenetic features (DNA modification, chromatin accessibility) of Treg cells are attenuated in the absence of Tet2 and Tet3. Conversely, the addition of the TET activator vitamin C during TGFβ-induced iTreg cell differentiation *in vitro* potentiates the expression of Treg signature genes and alters the epigenetic landscape to better resemble that of Treg cells generated *in vivo*. Vitamin C enhances IL-2 responsiveness in iTreg cells by increasing IL2Rα expression, STAT5 phosphorylation, and STAT5 binding, mimicking the IL-2/STAT5 dependence of Treg cells generated *in vivo*. In summary, TET proteins play essential roles in maintaining Treg molecular features and promoting their dependence on IL-2. TET activity during endogenous Treg development and potentiation of TET activity by vitamin C during iTreg differentiation are necessary to maintain the transcriptional and epigenetic features of Treg cells.

Keywords epigenetics; IL-2; STAT5 signaling; TET proteins; Treg cells; vitamin C

Subject Categories Chromatin, Transcription & Genomics; Immunology; Signal Transduction

DOI 10.15252/embr.202152716 | Received 19 February 2021 | Revised 15 June 2021 | Accepted 16 June 2021 | Published online 21 July 2021

EMBO Reports (2021) 22: e52716

Introduction

Enzymes of the TET family are Fe(II) and 2-oxoglutarate-dependent dioxygenases that catalyze sequential oxidation of the methyl group of 5-methylcytosine (5mC) in DNA to 5-hydroxymethylcytosine (5hmC) and the further oxidized products 5-formalcytosine (5fC) and 5-carboxylcytosine (5caC) (Iyer *et al*, 2009; Tahiliani *et al*, 2009; He *et al*, 2011; Ito *et al*, 2011). These modified bases are intermediates in DNA demethylation as well as potential epigenetic marks capable of recruiting reader proteins that exert specific functions (Pastor & Rao, 2013; Tsagaratou *et al*, 2017b; Wu & Zhang, 2017). There are three mammalian TET proteins, TET1, TET2, and TET3, of which TET2 and TET3 are most highly expressed in cells of the immune and hematopoietic systems (Tsagaratou & Rao, 2013). Like all Fe(II) and 2-oxoglutarate-dependent dioxygenases, TET enzymes utilize 2-oxoglutarate (2OG), Fe (II), and molecular oxygen to generate their oxidized products, with CO_2 and succinate formed as byproducts (Hausinger, 2004). The enzymatic activity of TET proteins can be modulated by diverse factors, including the ambient levels of oxygen (hypoxia versus normoxia) and diverse metabolic enzymes that regulate the intracellular levels of either 2OG itself or its competitive inhibitor 2-hydroxyglutarate (2HG) (Dang & Su, 2017; Lio & Rao, 2019; Lio *et al*, 2020). Both stereoisomers of 2HG are inhibitors of TET proteins and other dioxygenases, with the D (or *S*(+)) stereoisomer being significantly more potent than the L (or *R*(−)) form (Xu *et al*, 2011; Ye *et al*, 2018). In contrast, vitamin C (ascorbate) is a potent activator of TET proteins and other dioxygenases; it is believed to act by restoring the reduced state of Fe(II) at the dioxygenase active site in each catalytic cycle in which Fe(II) is converted to Fe(III) (Blaschke *et al*, 2013; Yue *et al*, 2016).

TET proteins are required to maintain the stability and function of regulatory T (Treg) cells, a distinct lineage of $CD4^+$ T cells that maintain immune self-tolerance and homeostasis (Sakaguchi *et al*, 2008; Josefowicz *et al*, 2012; Li & Zheng, 2015; Yang *et al*, 2015; Yue *et al*, 2016). T regulatory cells are defined by expression of the X-chromosome-encoded transcription factor FOXP3, a lineage-determining transcription factor essential for Treg development and function (Sakaguchi *et al*, 2008; Josefowicz *et al*, 2012; Li & Zheng, 2015). TET proteins also control the stability of FOXP3 expression

1 Division of Signaling and Gene Expression, La Jolla Institute for Immunology, La Jolla, CA, USA
2 Biological Sciences Graduate Program, University of California, San Diego, La Jolla, CA, USA
3 Bioinformatics and Systems Biology Program, University of California, San Diego, La Jolla, CA, USA
4 Sanford Consortium for Regenerative Medicine, La Jolla, CA, USA
5 Department of Hematology and Medical Oncology, Emory University School of Medicine, Atlanta, GA, USA
6 Department of Pharmacology and Moores Cancer Center, University of California, San Diego, La Jolla, CA, USA
*Corresponding author. Tel: +1 404 778 3875; E-mail: bbarwic@emory.edu
**Corresponding author. Tel: +1 858 952 7155; E-mail: arao@lji.org
†These authors contributed equally to this work

in "induced" regulatory T cells (iTreg cells), generated *in vitro* by activation of naïve CD4$^+$ T cells through the T-cell receptor (TCR) and the costimulatory receptor CD28 in the presence of TGFβ and/or retinoic acid (RA) (Yue *et al*, 2016). Both during thymic development and during iTreg differentiation, TET proteins are dispensable for the initial acquisition of FOXP3 expression, but are critical for maintaining the stability of FOXP3 expression through cell division *in vitro* and *in vivo* (Yang *et al*, 2015; Yue *et al*, 2016).

The stability of FOXP3 expression is regulated by the DNA methylation status of an intronic enhancer, *CNS2* (conserved noncoding sequence 2) located in the first intron of the *Foxp3* gene (Zheng *et al*, 2010; Feng *et al*, 2014b; Li *et al*, 2014). The 12 CpG sites in the mouse *Foxp3 CNS2* enhancer are predominantly "methylated" in iTreg cells generated with TGFβ or TGFβ and RA but predominantly "unmethylated" in endogenous Treg cells (Floess *et al*, 2007; Huehn *et al*, 2009; Toker & Huehn, 2011); the words "methylated" and "unmethylated" are in quotation marks because bisulfite sequencing does not distinguish 5mC and 5hmC, or unmodified cytosine from 5fC and 5caC (Huang *et al*, 2010). Notably, deletion of the *Tet2* and *Tet3* genes with either *CD4Cre* or *Foxp3Cre* during Treg development results in increased methylation of *Foxp3 CNS2* in *Tet2/3* DKO Treg cells compared with WT Treg cells and a marked defect in Foxp3 stability (Yue *et al*, 2016; Yue *et al*, 2019). In a parallel gain-of-function approach, we have shown that addition of the TET activator vitamin C during *in vitro* iTreg differentiation leads to TET-dependent demethylation of *Foxp3 CNS2* and a substantial increase in Foxp3 stability after adoptive transfer *in vivo* or cell division *in vitro* (Sasidharan Nair *et al*, 2016; Yue *et al*, 2016).

To gain a better understanding of the role of TET dioxygenases in Treg function, we embarked on genome-wide analyses to compare wild-type (WT) CD4$^+$ naïve T cells with endogenous WT Treg cells and *Tet2/3*-deficient Treg cells. In parallel, we used the gain-of-function approach to document the genome-wide effects of vitamin C on iTreg differentiation, comparing iTreg cells generated by activation in the presence of TGFβ alone or TGFβ plus retinoic acid (RA) with cells generated under the same conditions but with vitamin C added to the culture medium. We assessed (i) transcriptional profiles (by RNA-sequencing, RNA-seq); (ii) 5hmC distribution (by CMS-IP, DNA immunoprecipitation with antibodies to cytosine 5-methylenesulphonate (CMS), the product of 5hmC after bisulfite treatment (Pastor *et al*, 2011; Huang *et al*, 2012)); (iii) genome-wide DNA methylation patterns (by whole-genome bisulfite sequencing, WGBS); and (iv) the chromatin accessibility landscape (by assay for transposase-accessible chromatin using sequencing, ATAC-seq). We find that in the absence of Tet2 and Tet3, Treg cells fail to maintain Treg-specific epigenetic features and the expression of Treg signature genes. Moreover, the changes induced by vitamin C during TGFβ-induced iTreg differentiation *in vitro* resemble those occurring in a TET-dependent manner in endogenous Tregs *in vivo*, although the *in vitro* effects of vitamin C on iTreg differentiation are, as expected, less striking than the differences between WT and TET-deficient Tregs generated *in vivo*. TET deletion *in vivo* resulted in impaired IL2/STAT5 signaling, while boosting TET activity with vitamin C enhanced IL-2 responsiveness in iTreg cells by increasing IL2Rα expression and STAT5 activity. Our study provides compelling evidence for manipulation of TET activity in future Treg-mediated treatment of autoimmune disease.

Results

Dysregulation of gene expression patterns in Treg cells in the absence of Tet2 and Tet3

To examine the transcriptional changes in Treg cells upon *Tet2* and *Tet3* deletion, we performed RNA-seq on WT Treg cells, *Tet2/Tet3*-deficient Treg cells, and WT CD4$^+$ naïve T cells. Floxed exons 8-10 of *Tet2* and exon 2 of *Tet3* were efficiently deleted in Treg cells isolated from *Tet2*$^{fl/fl}$*Tet3*$^{fl/fl}$*CD4Cre* (*Tet2/3* DKO) mice (Yue *et al*, 2016; Tsagaratou *et al*, 2017a) compared with WT Treg cells, as shown by RNA-seq (Appendix Fig S1A). Principal component analysis of gene expression data showed that samples clustered by cell type: CD4$^+$ naïve T-cell replicates clustered together, as did replicates for WT and *Tet2/3* DKO Treg cells (Fig 1A). Principal component 1 (PC1) distinguished CD4$^+$ naïve T cells from both WT Treg and *Tet2/3* DKO Treg cells, whereas principal component 2 (PC2) separated WT Treg cells from *Tet2/3* DKO Treg cells (Fig 1A). Differential analysis showed that 2,245 genes were differentially expressed in WT Treg cells compared with CD4$^+$ naïve T cells, while 614 genes were differentially expressed in WT Treg compared with *Tet2/3* DKO Treg cells (Fig 1B, Dataset EV1).

Gene Set Enrichment Analysis (GSEA) of Hallmark gene sets (Subramanian *et al*, 2005; Liberzon *et al*, 2015) showed that the IL-2/STAT5 signaling gene set was highly enriched in WT Treg cells compared with CD4$^+$ naïve T cells as expected (Fig 1C, *upper panel*), since the IL-2/STAT5 signaling axis is essential for the functional programming of Treg cells and the maintenance of immune homeostasis (Ross & Cantrell, 2018). The IL2/STAT5 signaling gene set was also highly enriched in WT Treg cells compared with *Tet2/3* DKO Treg cells (Fig 1C, *lower panel*). Consistent with the gene expression changes, the expression of IL2Rα (CD25) was reduced in *Tet2/3* DKO Treg cells compared with WT Treg cells (Appendix Fig S2A), as well as the phospho-STAT5 levels upon IL-2 restimulation (Appendix Fig S2B). These data suggested that TET deletion led to impaired IL-2/STAT5 signaling. We also found that the E2F Target gene set, which includes genes essential for DNA replication and cell cycle and is one of the most frequently altered pathway categories upon TET deletion (Tsagaratou *et al*, 2017a; Yue *et al*, 2019), was highly enriched in *Tet2/3* DKO Treg cells compared with WT Treg cells (Fig 1D, *lower panel*).

We also examined the representation of Treg signature genes from Hill *et al* (2007) using GSEA. Treg signature genes upregulated in Treg cells compared with conventional T cells (Hill *et al*, 2007) were significantly enriched in WT Treg cells compared with CD4$^+$ naïve T cells as expected (Fig 1E, *upper panel*) but were significantly depleted in *Tet2/3* DKO Treg compared with WT Treg cells (Fig 1E, *lower panel*). Conversely, Treg signature genes downregulated in Treg cells compared with conventional T cells (Hill *et al*, 2007) were significantly depleted in WT Treg cells compared with CD4$^+$ naïve T cells (Appendix Fig S1B, *upper panel*) but were evenly distributed between WT Treg and *Tet2/3* DKO Treg cells (Appendix Fig S1B, *lower panel*). These data suggested that TET proteins are more involved in activation of Treg signature genes than in their suppression. Selected Treg signature genes—*Foxp3*, *Il10ra*, *Nrp1*, *Ikzf4*, and *Ccr6*—are shown in Fig 1F; their expression levels were lower in *Tet2/3* DKO Treg than in WT Treg cells, except for *Foxp3*, which was used as a marker for Treg cell isolation. The

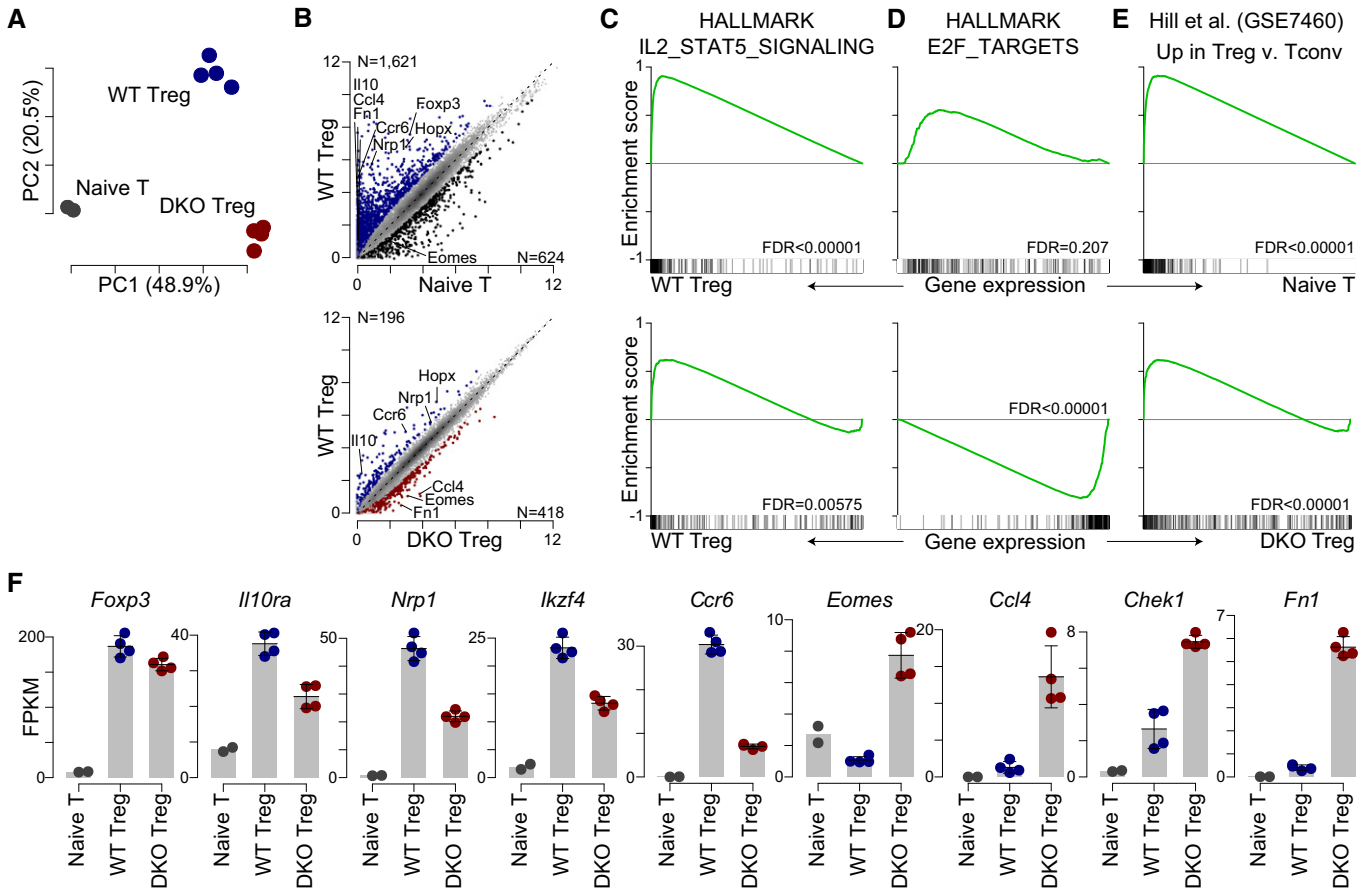

Figure 1. Dysregulated transcriptional program in Treg cells in the absence of *Tet2* and *Tet3*.

A Principal component analysis of WT CD4$^+$ naïve T cells (*gray*), WT Treg cells (*blue*), and *Tet2/3* DKO Treg cells (*red*). The percent of variation explained by principle components 1 (PC1) and 2 (PC2) are shown in parenthesis.

B Scatter plots showing the comparison of mean gene expression between WT Treg cells versus CD4$^+$ naïve T cells (*upper panel*) and WT Treg cells versus *Tet2/3* DKO Treg cells (*lower panel*). Differentially expressed genes (FDR $\leq$ 0.05 and fold-change $\geq$ 2) are shown in color (*blue*: WT Treg cells; *black*: CD4$^+$ naïve T cells; *red*: *Tet2/3* DKO Treg cells), and selected genes are labeled in the plots. The scale is $\log_2$(FPKM+1).

C–E Gene Set Enrichment Analysis of gene expression changes between WT Treg cells versus CD4$^+$ naïve T (*upper panels*) and WT Treg cells versus *Tet2/3* DKO Treg cells (*lower panels*) for the Hallmark gene sets IL-2/STAT5 signaling (C), E2F Target genes (D), and Treg signature gene set that are upregulated in Treg cells compared with conventional T cells (GSE7460) (E). The green line represents the enrichment score with enrichment in WT Treg cells shown to the left and enrichment in CD4$^+$ naïve T (*upper panels*) or Tet2/3 DKO Treg cells (*lower panels*) shown to the right. Overlap of genes in the given gene set is shown below and denoted by black ticks.

F Examples of expression levels of Treg signature genes *Foxp3*, *Il10ra*, *Nrp1*, *Ikzf4*, and *Ccr6*; and examples of expression levels of genes upregulated in *Tet2/3* DKO Treg cells *Eomes*, *Ccl4*, *Chek1*, and *Fn1*. The y-axis shows FPKM (Fragment Per Kilobase per Million reads), and the x-axis shows the different cell types. Error bars show mean $\pm$ SD from two (CD4$^+$ naïve T cells) or four (WT and *Tet2/3* DKO Treg) biological replicates.

expression levels of genes related to the effector program, cell cycle and cell adhesion—*Eomes*, *Ccl4*, *Chek1*, and *Fn1*—were dramatically increased upon TET deletion (Fig 1F). Together, these data show clearly that the transcriptional program of Treg cells is altered upon TET deletion; specifically, *Tet2/3* DKO Treg cells show notably impaired expression of genes in the Treg signature program.

5hmC distribution correlates strongly with gene expression levels

WT Treg cells and CD4$^+$ naïve T cells have similar amounts of genomic 5hmC, as assessed by dot blot of sodium bisulfite-treated DNA with antibodies recognizing cytosine 5-methylenesulphonate (CMS), the product of 5hmC after bisulfite treatment (Pastor *et al*, 2011; Huang *et al*, 2012) (Fig 2A). This was also reflected in the similar numbers of 5hmC-marked regions enriched over input in CD4$^+$ naïve T cells and WT Treg cells based on immunoprecipitation (CMS-IP) of genomic DNA with anti-CMS (Appendix Fig S3A and B). 12,279 5hmC-marked regions were differentially hydroxymethylated between these two cell types (Treg > naïve, 9,058 regions, naïve > Treg, 3,221 regions; Fig 2B, Dataset EV2). Compared with the mm9 genome, 5hmC was depleted in intergenic regions but significantly enriched at promoter regions ($\pm$1 kb of TSS) and in transcribed regions of genes—introns, exons, 5′ and 3′ UTRs, and transcription termination sites (Appendix Fig S3C and D). 5hmC levels were also low at transcription start sites (TSS) (Appendix Fig S3E) because these regions have lower levels of the substrate 5mC ((Tsagaratou *et al*, 2017a); also see Fig EV1B below). However, 5hmC levels in the latter two-thirds of gene bodies showed a very

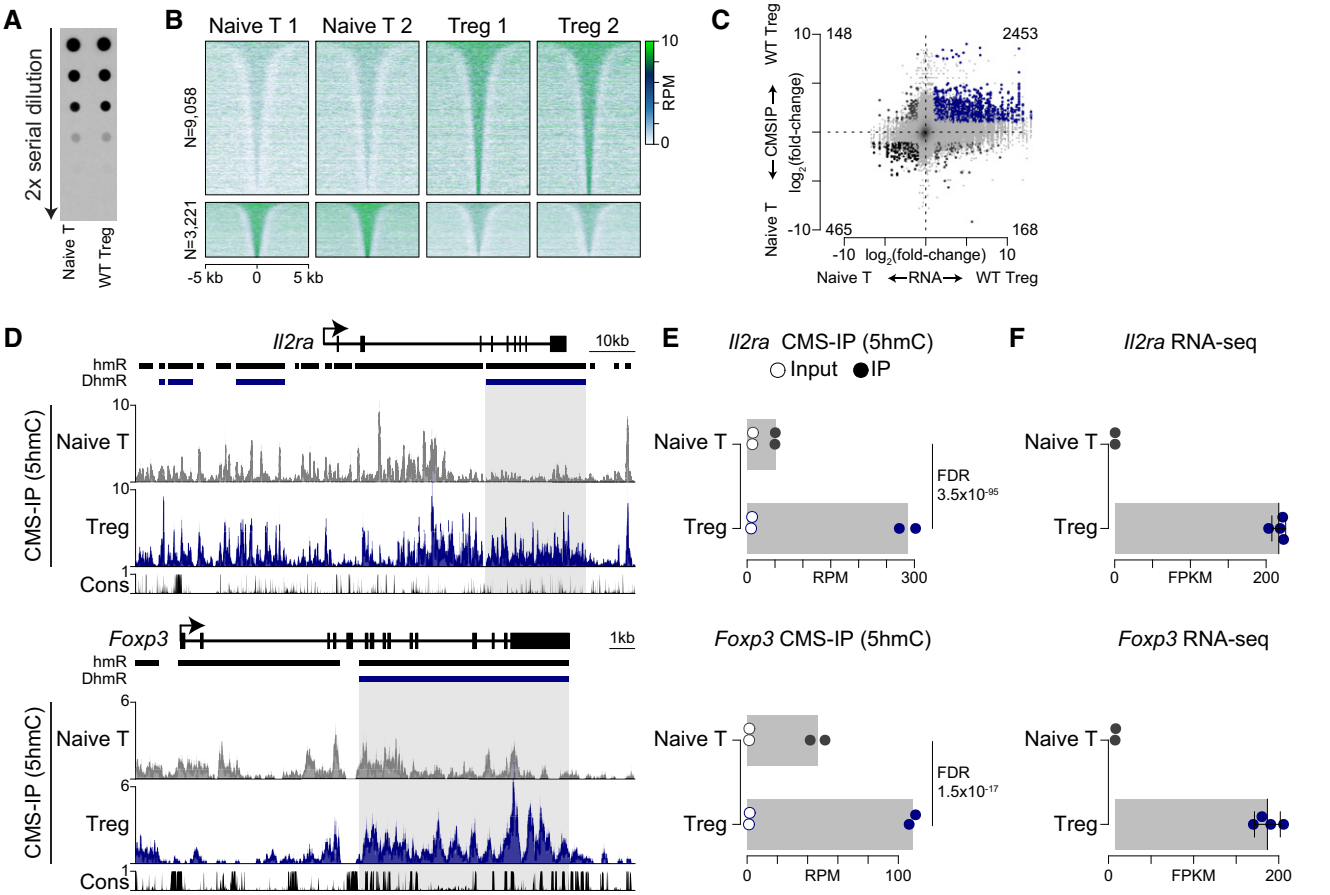

Figure 2. 5hmC correlates with gene expression.

A Anti-CMS dot blot assay assessing the global amount of 5hmC levels in CD4$^+$ naïve T cells and WT Treg cells. Data are representative of three biological replicates.

B Heat maps of differentially hydroxymethylated regions (DhmRs) between CD4$^+$ naïve T cells and WT Treg cells.

C Scatter plot of 5hmC changes (y-axis) and gene expression changes (x-axis) between CD4$^+$ naïve T and WT Treg cells. DhmRs associated with a differentially expressed gene are denoted in color (*blue*: WT Treg cells; *black*: CD4$^+$ naïve T cells).

D Genome browser view of CMS-IP data showing CMS (5hmC) distribution at *Il2ra* and *Foxp3* locus for CD4$^+$ naïve T cells and WT Treg cells. Hydroxymethylated regions (hmRs) and DhmRs are shown on the top; conservation (cons) is shown at the bottom.

E The graphs show CMS (5hmC) signal (RPM) in DhmRs denoted by the shaded region in D for IP and Input in CD4$^+$ naïve T cells and WT Treg cells. FDRs are calculated based on the Benjamini–Hochberg correction of *P*-values determined using a negative binomial distribution (see methods). Error bars show mean ± SD from two biological replicates.

F The graphs show the expression levels of *Il2ra* (*upper panel*) and *Foxp3* (*lower panel*) in CD4$^+$ naïve T cells and WT Treg cells. Error bars show mean ± SD from two (CD4$^+$ naïve T cells) or four (WT Treg) biological replicates.

good correlation with gene expression: As shown for other cell types (Tsagaratou *et al*, 2014; Tsagaratou *et al*, 2017a), the greatest amounts of 5hmC were present in the gene bodies of the highest expressed genes in both CD4$^+$ naïve T cells and WT Treg cells (Appendix Fig S3E).

We examined the relation of differentially hydroxymethylated regions (DhmRs) to differentially expressed genes (DEGs) and found that DhmRs that were more hydroxymethylated in WT Treg cells (Treg-specific DhmRs) were significantly associated with DEGs expressed at higher levels in WT Treg cells compared with CD4$^+$ naïve T cells (Fig 2C, *blue dots*). Conversely, DhmRs that were more hydroxymethylated in CD4$^+$ naïve T cells (naïve T cell-specific DhmRs) were significantly associated with DEGs expressed at higher levels in CD4$^+$ naïve T cells compared with WT Treg cells (Fig 2C, *black dots*). This point is illustrated by the genome browser tracks and quantified 5hmC signal for the *Foxp3* and *Il2ra* genes (Fig 2D and E); again, integrated 5hmC levels in the latter part of gene bodies correlated well with levels of gene expression (Fig 2F).

These data highlight the strong correlation of 5hmC levels with gene expression, cell differentiation, and lineage specification, as previously noted for other immune and non-immune cell types (Neri *et al*, 2013; Tsagaratou *et al*, 2014; Tsagaratou *et al*, 2017a). We note, however, that despite showing the expected profound loss of 5hmC (Yue *et al*, 2016), *Tet2/3* DKO Treg cells show equivalent expression of many genes compared with WT Treg cells (Fig 1B), indicating that 5hmC modulates gene expression rather than driving gene transcription.

Treg-specific DNA demethylation patterns are impaired in the absence of Tet2 and Tet3

Because our data suggested that TET proteins were important for correct specification of the full Treg signature program during Treg differentiation, we interrogated the effects of TET deletion on DNA methylation by whole-genome bisulfite sequencing (WGBS) to identify CpGs that were differentially modified in naïve CD4$^+$ T cells, WT, and *Tet2/3* DKO Treg cells (Fig 3). Bisulfite sequencing cannot distinguish 5mC and 5hmC, and therefore reports on the sum of 5mC+5hmC; nevertheless, since 5hmC is typically <5-10% of 5mC, the data are often termed "methylation" for convenience. Principal component analysis of DNA methylation data showed that CD4$^+$ naïve T-cell replicates clustered together, as did replicates for WT and *Tet2/3* DKO Treg cells; principal component 1, which distinguished naïve CD4$^+$ T cells from WT Treg cells as well as WT Treg

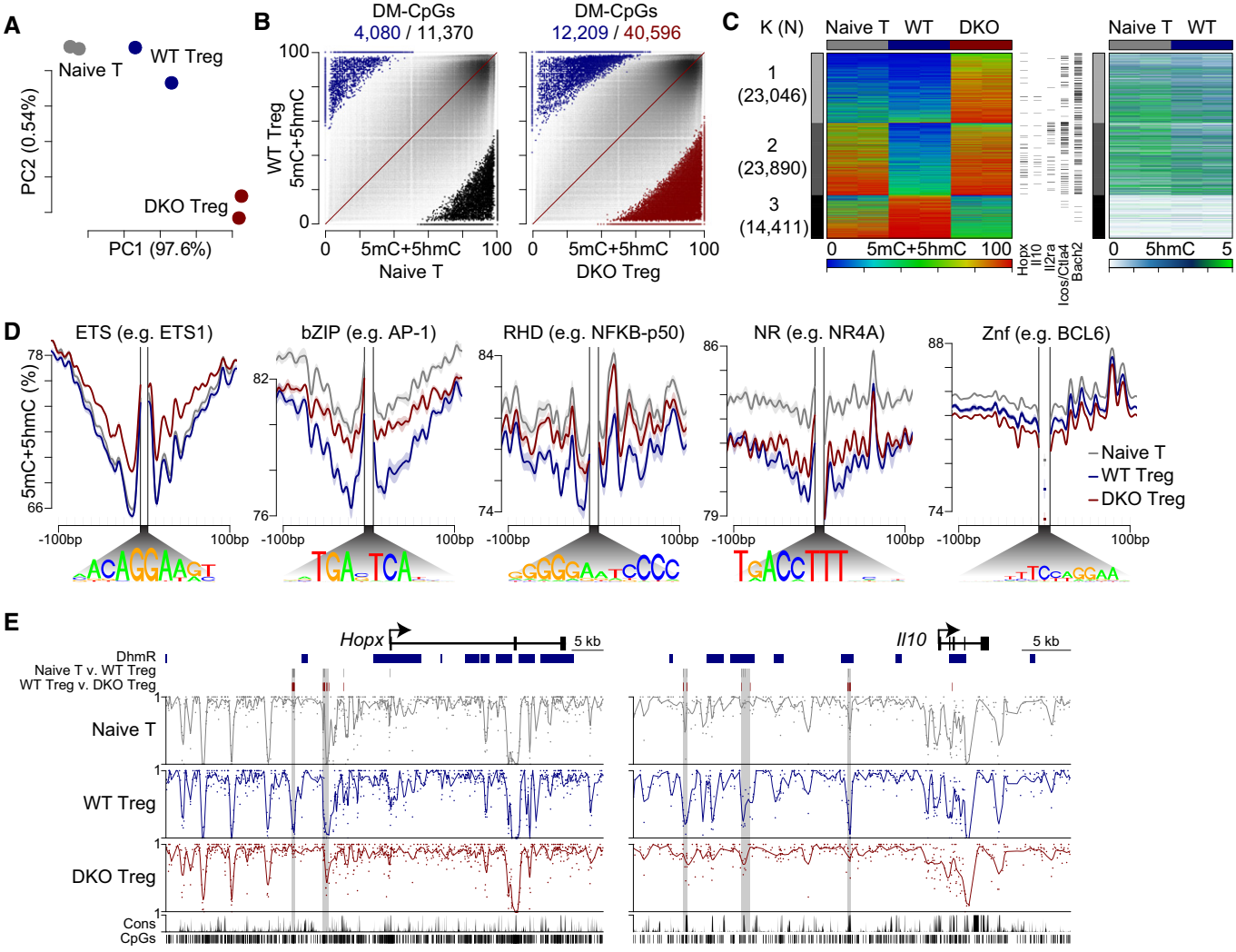

Figure 3. Treg-specific DNA demethylation patterns are impaired in the absence of Tet2 and Tet3.

A Principal component analysis of DNA methylation data at 17,937,401 CpGs for CD4$^+$ naïve T cells (*gray*), WT Treg cells (*blue*) and *Tet2/3* DKO Treg cells (*red*). The percentage of variation explained by each component is shown in parentheses.

B Scatter plots of DNA methylation data showing the comparisons between WT Treg versus CD4$^+$ naïve T cells (*left*) and WT Treg versus *Tet2/3* DKO Treg cells (*right*). The differentially methylated CpGs (DM-CpGs) are shown in color (*blue*: WT Treg; *black*: CD4$^+$ naïve T cells; *red*: *Tet2/3* DKO), and the numbers are shown on top of each graph.

C K-means clustering of DNA methylation data for all the samples using CpGs differentially methylated between CD4$^+$ naïve T cells versus WT Treg cells and WT Treg versus *Tet2/3* DKO Treg cells (*left*); the number (N) of CpGs in each cluster is shown in parenthesis. *Middle*: CpG loci proximal to selected genes are annotated. *Right*: the average DNA hydroxymethylation levels at each CpGs as measured by CMS-IP.

D The average DNA methylation levels at selected consensus transcription factor-binding motifs (*gray*: CD4$^+$ naïve T cells; *blue*: WT Treg cells; *red*: *Tet2/3* DKO Treg cells). Standard error is denoted in transparency of the corresponding colors.

E Genome browser view of DNA methylation patterns of *Hopx* and *Il10* loci for CD4$^+$ naïve T cells, WT Treg cells and *Tet2/3* DKO Treg cells. Differentially hydroxymethylated regions (DhmRs) and differentially methylated CpGs (DM-CpGs) are shown on top of the tracks. Conservation track (Cons) and denotation of all CpGs are shown at the bottom. WGBS data are from two biological replicate samples.

cells from *Tet2/3* DKO Treg cells, represented the majority of the variation (97.6%) whereas principal component 2 only separated WT Treg cells from *Tet2/3* DKO Treg cells (Fig 3A). Global CpG methylation levels were very similar in all three cell types (Fig EV1A). As previously noted by our own and other groups (Lee *et al*, 2002; Laurent *et al*, 2010; Tsagaratou *et al*, 2017a), the most highly expressed genes in each cell type showed prominent demethylation at promoter/TSS regions, and this demethylation extended well into the gene body (Fig EV1B).

We then analyzed the differentially methylated CpGs (DM-CpGs) (Dataset EV3). Comparing $CD4^+$ naïve T cells and WT Treg cells, the majority of the DM-CpGs (11,370/15,450; 73.6%) were more methylated in naïve $CD4^+$ T cells (Fig 3B, *left panel*). Similarly, comparing *Tet2/3* DKO with WT Treg cells, most of the 52,805 DM-CpGs (76.9%) were more methylated in the *Tet2/3* DKO cells as expected (Fig 3B, *right panel*). K-means clustering of DM-CpGs in selected pairwise comparisons ($CD4^+$ naïve T versus WT Treg and WT Treg versus *Tet2/3* DKO Treg) identified clusters with distinct DNA methylation patterns among the cell types (Fig 3C, *left panel*). Cluster 1 contained ~23,000 DM-CpGs whose demethylated status, at least in mature Treg cells, was maintained by Tet2 and/or Tet3; these CpGs were demethylated in both $CD4^+$ naïve T cells and WT Treg cells, but showed increased DNA methylation in *Tet2/3* DKO Treg cells. Cluster 2 contained ~24,000 DM-CpGs that showed Treg-specific, TET-regulated DNA methylation patterns: The majority of these CpGs were highly methylated in $CD4^+$ naïve T cells and became demethylated in WT Treg cells, but remained highly methylated in *Tet2/3* DKO Treg cells (Fig 3C, *left panel*). Notably, both CpG clusters 1 and 2 were marked by a significant amount of 5hmC in both $CD4^+$ naïve T cells and WT Treg cells, confirming that TET proteins act directly to oxidize 5mC at these CpG sites (Fig 3C, *right panel*). In contrast, cluster 3 contained ~14,000 DM-CpGs that showed increased DNA methylation in WT Treg cells compared with $CD4^+$ naïve T cells and *Tet2/3* DKO Treg cells (Fig 3C, *left panel*). Notably, this cluster was depleted for 5hmC in both $CD4^+$ naïve T cells and WT Treg cells (Fig 3C, *right panel*). We speculate that the CpGs in this cluster reside in heterochromatin, perhaps in genes or regions that are repressed during the course of Treg differentiation, since they are highly methylated in WT Treg cells but undergo a paradoxical loss (rather than the expected gain) of DNA methylation in TET-deficient Treg cells (Lopez-Moyado *et al*, 2019). We then annotated the CpGs in each K-means cluster using Genomic Regions Enrichment of Annotations Tool (GREAT) (McLean *et al*, 2010). The results showed that CpGs in clusters 1 and 2 are proximal to genes regulating immune responses, lymphocyte cell activation, and cell adhesion (Dataset EV4; CpGs proximal to the selected genes were annotated in Fig 3C, *middle panel*). In contrast, CpGs in cluster 3, which were aberrantly demethylated in *Tet2/3* DKO Treg cells, were associated with genes regulating amino acid transport (Dataset EV4).

We assessed DNA methylation (5mC+5hmC) levels at selected consensus transcription factor (TF) binding sites ($\pm$ 100 bp, centered on the sites; Dataset EV5). DNA methylation levels surrounding consensus ETS-binding motifs were lower in both $CD4^+$ naïve T cells and WT Treg cells compared with *Tet2/3* DKO Treg cells, consistent with the well-established roles of ETS family members in T-cell activation and Treg development and function (Muthusamy *et al*, 1995; Mouly *et al*, 2010; Luo *et al*, 2017) (Fig 3D, *left*). DNA methylation levels surrounding consensus binding motifs for members of the basic region-leucine zipper (bZIP), Rel-homology domain (RHD), and nuclear receptor (NR) transcription factor families were predominantly located in CpG cluster 2, i.e., Treg-specific (methylation levels lower in WT Treg cells compared with $CD4^+$ naïve T cells) as well as TET-regulated (methylation levels higher in *Tet2/3* DKO Treg cells compared with WT Treg cells) (Fig 3D, *middle*). These transcription factor families, including JunB, BATF, BACH2 (bZIP), NFAT, NFκB RelA and c-Rel (RHD) and NR4A (NR), are all important regulators of Treg development and function (Wu *et al*, 2006; Roychoudhuri *et al*, 2013; Sekiya *et al*, 2013; Grinberg-Bleyer *et al*, 2017; Hayatsu *et al*, 2017; Koizumi *et al*, 2018; Ronin *et al*, 2019). Consistent with these data, motif enrichment analysis of DhmRs showed that consensus binding sequences of transcription factors ETS and ETS:RUNT composite motifs were enriched in DhmRs specific to naïve T cells, whereas consensus binding sequences of bZIP, RHD, and NR families were enriched in Treg-specific DhmRs (Fig EV1C, Dataset EV6). In contrast, DNA methylation levels at consensus zinc finger (Znf) transcription factor-binding sites displayed a different pattern: Methylation levels were comparable or even lower in *Tet2/3* DKO Treg cells compared with WT Treg cells (Fig 3D, *right*).

Genome browser views of DNA methylation levels at the *Hopx* and *Il10* loci showed Treg-specific and TET-regulated DM-CpGs (Fig 3E). Many of these overlapped or were adjacent to Treg-specific DhmRs, as especially apparent at the *Il10* locus (Figs 3E and EV1D, *gray shaded regions*). The *Cd28/Ctla4/Icos*, *Il2ra*, and *Bach2* loci also displayed stretches of CpGs with Treg-specific and TET-regulated methylation patterns (Fig EV1E), again mainly located in CpG cluster 2 (Fig 3C).

Together these data suggest that TET proteins have a critical role in maintaining Treg-specific demethylated CpGs. Moreover, motifs displaying Treg-specific TET-regulated methylation patterns correlated well with motifs enriched at Treg-specific DhmRs.

Chromatin accessibility patterns of Treg cells in the absence of Tet2 and Tet3

Analysis of chromatin accessibility by ATAC-seq (Buenrostro *et al*, 2013), followed by principal component analysis, again showed that samples from naïve $CD4^+$ T cells, WT Treg cells, and *Tet2/3* DKO Treg cells clustered by cell type (a published ATAC-seq dataset was used for the naïve $CD4^+$ T cells (Yoshida *et al*, 2019)); again, the differences between $CD4^+$ naïve T cells and Treg cells, either WT or *Tet2/3* DKO, were more striking than the differences between WT and *Tet2/3* DKO Treg cells, accounting for 47% and 18% of the variability, respectively (shown as principal components 1 and 2, PC1 and PC2, in Fig 4A). Of 3,471 regions showing altered accessibility, 2,270 regions were more accessible and 1,201 regions were less accessible in WT compared with *Tet2/3* DKO Treg cells (Fig 4B, Dataset EV7). K-means clustering of the 3,471 regions identified clusters with distinct patterns of accessibility changes (Fig 4C): regions that lost accessibility in *Tet2/3* DKO Treg cells compared with both $CD4^+$ naïve T cells and WT Treg cells (cluster 1); regions that were more accessible in WT Treg cells compared with $CD4^+$ naïve T cells (Treg-specific) and whose accessibility decreased upon TET deletion (TET-regulated) (cluster 2); regions that were more accessible in *Tet2/3* DKO Treg cells compared with both naïve $CD4^+$

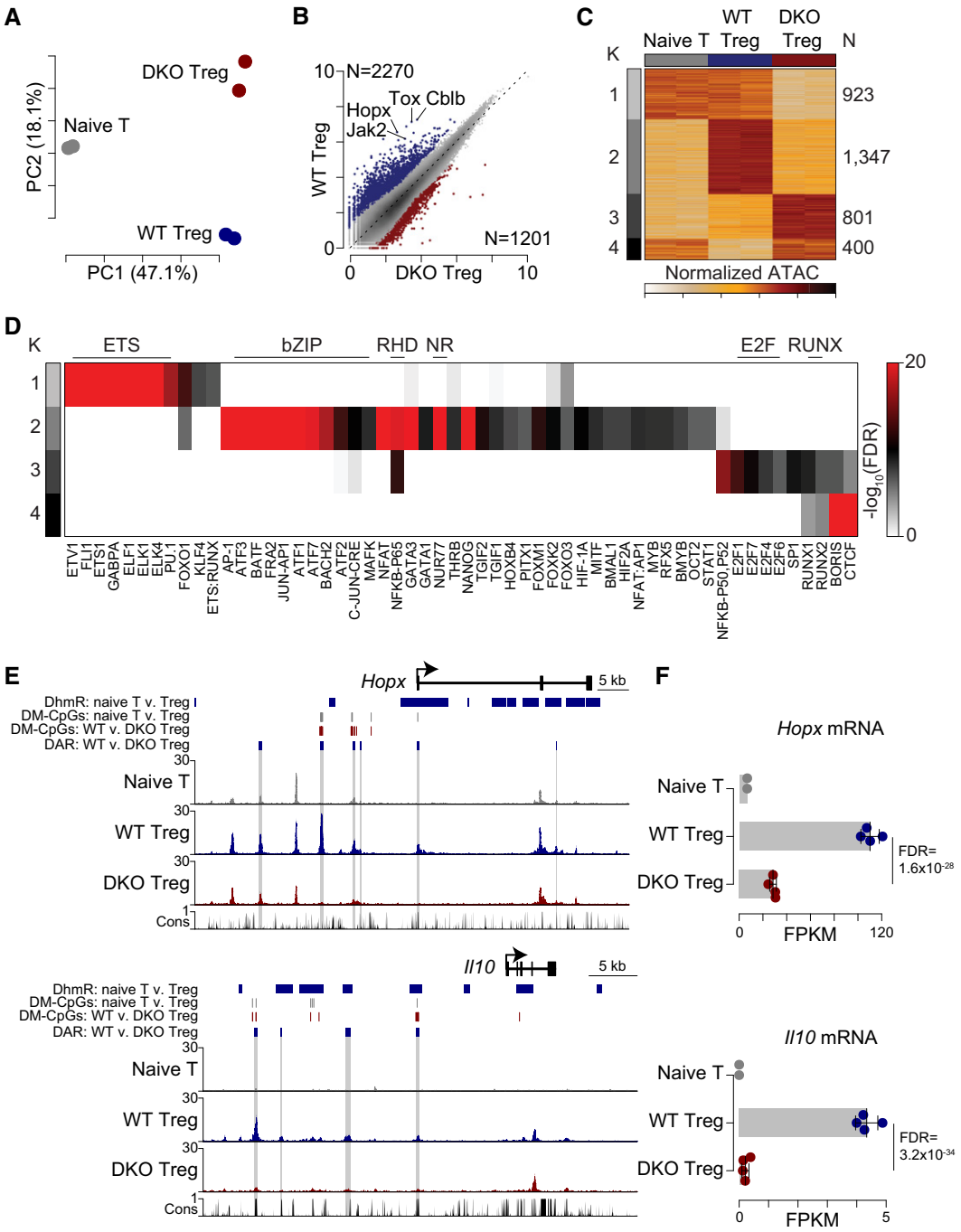

Figure 4. Changes of chromatin accessibilities in the absence of Tet2 and Tet3.

A Principal component analysis of WT CD4$^+$ naïve T cells (*gray*), WT Treg cells (*blue*), and *Tet2/3* DKO Treg cells (*red*). The percent of variation explained by principle components 1 (PC1) and 2 (PC2) are shown in parenthesis.

B Scatter plot of ATAC-seq data for WT Treg versus *Tet2/3* DKO Treg cells. Differentially accessible regions (DARs) are shown in color, and the total number of DARs (N) is shown on the graph.

C K-means clustering of ATAC-seq data for DARs between WT Tregs and *Tet2/3* DKO Tregs. ATAC-seq data for CD4$^+$ naïve T cells is from Yoshida *et al* (2019). The number of regions in each cluster is denoted.

D Heat map of transcription factor-binding motifs in each K-means cluster. The significance of enrichment (−log10(FDR)) is denoted by color scale. Transcription factor families of particular interest are highlighted on top of the heat map.

E Genome browser view of chromatin accessibilities at *Hopx* and *Il10* loci for CD4$^+$ naïve T cells, WT Treg cells, and *Tet2/3* DKO Treg cells. DhmRs, DM-CpGs, and DARs (*shaded*) are shown on top of the tracks. Conservation track (Cons) is shown at the bottom.

F Expression levels of *Hopx* and *Il10* in CD4$^+$ naïve T cells, WT Treg cells, and *Tet2/3* DKO Treg cells. Error bars show mean ± SD from two biological replicate samples.

T cells and WT Treg cells (cluster 3); and regions that were similarly accessible in naïve CD4$^+$ T cells and *Tet2/3* DKO Treg cells but which lost accessibility in WT Treg cells (cluster 4).

Motif analysis of regions in each cluster (Fig 4D, Dataset EV8) showed enrichment for consensus ETS-binding motifs in cluster 1, corresponding with the previously noted increase in DNA methylation levels at ETS-binding sites in *Tet2/3* DKO Treg cells compared with naïve CD4$^+$ T cells and WT Treg cells (Fig 3D, *left*). Similarly, RHD, bZIP, and NR binding motifs were enriched in cluster 2, which contained Treg-specific TET-regulated accessible regions, again consistent with the Treg-specific TET-regulated DNA methylation patterns at these transcription factor-binding sites (Fig 3D, *middle*). These patterns are illustrated in genome browser views of chromatin accessibilities at the *Hopx* and *Il10* loci (Fig 4E), which in many cases overlapped with Treg-specific TET-regulated methylation patterns (Fig 3E), and corresponded well with gene expression changes among the three cell types (Fig 4F).

The *Tiam1*, *Tox*, and *Rpl24* loci also displayed Treg-specific and TET-regulated accessible regions (Appendix Fig S4A–C, *left panels*). The accessibility changes corresponded well with gene expression changes for Tiam1 and Tox; however, as expected for a component of the ribosome 60S subunit, Rpl24 was constitutively expressed in all three cell types (Appendix Fig S4A–C, *right panels*). As previously reported, the *CNS2* enhancer in the *Foxp3* locus is already accessible in Treg precursor cells (Samstein *et al*, 2012), and its accessibility was only slightly diminished in *Tet2/3* DKO compared with WT Treg cells (Appendix Fig S4D, *left panel*). *Foxp3* expression was only slightly reduced in *Tet2/3* DKO compared with WT Treg cells (Appendix Fig S4D, *right panel*; also see Fig 1F).

Overall, our results indicate that as with the transcriptional, 5hmC and WGBS changes described in previous sections, Treg-specific chromatin accessibility was significantly diminished in the absence of Tet2 and Tet3.

Vitamin C enhances Treg molecular features in iTreg cells differentiating *in vitro*

Vitamin C is a well-established activator of TET proteins and other iron- and α-ketoglutarate-dependent dioxygenases (Blaschke *et al*, 2013; Yue & Rao, 2020). We previously showed that compared with iTreg cells differentiated with TGFβ alone, iTreg cells differentiated with TGFβ and vitamin C showed demethylation of *CNS1* and *CNS2*, two intronic enhancers within the *Foxp3* locus, and increased the mean fluorescent intensity (MFI) and stability of Foxp3 expression (Yue *et al*, 2016). Tet2 and Tet3 were major targets of vitamin C in iTreg cells since both *CNS2* demethylation and Foxp3 MFI increase were abolished in vitamin C-treated *Tet2/3 DKO* iTreg cells using an ERT2-Cre-inducible system (Yue *et al*, 2016). We observed similar effects in *Tet2/3 DKO* iTreg cells mediated by CD4Cre: Vitamin C treatment increased the MFI of Foxp3 expression in WT iTreg cells but not in *Tet2/3* DKO iTreg cells (Appendix Fig S5). To determine whether vitamin C could potentiate Treg signatures in differentiating iTreg cells, we analyzed Th0 cells activated with anti-CD3 and anti-CD28 in the absence of any polarizing cytokines or neutralizing anti-cytokine antibodies, and iTreg cells activated with anti-CD3 and anti-CD28 and differentiated under four distinct conditions: TGFβ alone; TGFβ + vitamin C (VitC); TGFβ + retinoic acid (RA); and TGFβ + RA + VitC (referred to as Th0; TGFβ; VitC; RA; and RA + VitC for simplicity). We assessed gene transcription and chromatin accessibility changes in these cells by RNA-seq and ATAC-seq; additionally, since RA alone has little or no effect on demethylation of *Foxp3 CNS1* and *CNS2* (Yue *et al*, 2016), we examined 5hmC and DNA methylation changes by CMS-IP and WGBS in iTreg cells differentiated with TGFβ versus TGFβ + RA + VitC.

Hierarchical clustering of gene expression data showed that the samples clustered by cell type (Fig EV2A). K-means clustering of 713 genes differentially expressed in selected pairwise comparisons

Figure 5. Vitamin C promotes Treg molecular features in TGFβ-induced iTreg cells.

A K-means clustering of gene expression data for Th0 cells and iTreg cells differentiated *in vitro* under the conditions of TGFβ alone, TGFβ + VitC, TGFβ + RA; TGFβ + RA + VitC using genes differentially expressed between the pairwise comparisons indicated by the arrows on top of the heat map. The number of genes in each cluster is shown on the left.

B Gene Set Enrichment Analysis (GSEA) of expression changes induced by vitamin C treatment, for genes upregulated in Treg cells versus conventional T cells (GSE7460, *left panel*), genes upregulated in WT Treg cells versus CD4$^+$ naïve T cells (our data, *middle panel*), and genes upregulated in WT Treg cells versus *Tet2/3* DKO Treg cells (our data, *right panel*), presented as enrichment score (y-axis) and overlap of genes from each set (x-axis, shown on the bottom) with genes expressed higher in TGFβ + VitC and TGFβ + RA + VitC compared with TGFβ alone and TGFβ + RA, respectively. Data are from two biological replicates.

C K-means clustering of chromatin accessibility data (ATAC-seq) for Th0 cells and *in vitro* differentiated iTregs using regions differentially accessible between the pairwise comparisons indicated by the arrows on top of the heat map. The number of regions is shown on the left, and data are represented as normalized log2 (RPM+1).

D Scatter plot of ATAC-seq data for TGFβ + VitC versus TGFβ iTregs (*left*), TGFβ + RA + VitC versus TGFβ + RA iTregs (*middle*), and TGFβ + RA + VitC versus TGFβ iTregs (*right*). Differentially accessible regions (DARs) are shown in color, and the total number of DARs (N) are shown on each graph.

E Genome browser view of ATAC-seq data showing the accessibility profile at the *Foxp3* locus; the *CNS2* region is highlighted (*gray shading*). DARs are denoted above the cell type tracks with regions of more accessibility identified by color. Scale is reads per million (RPM), and conservation track (Cons) is shown at the bottom.

F Beeswarm plots of mean chromatin accessibility measured as log2 (RPM+1) for regions more accessible in TGFβ + VitC versus TGFβ (*left*) and TGFβ + RA + VitC versus TGFβ + RA (*right*). DARs denote the regions in the respective cell types used for the comparison and are indicated by the gray shading. *P*-values are calculated using an analysis of variances with Tukey's post hoc test and DARs are determined using a negative binomial test with Benjamini–Hochberg correction FDR ≤ 0.05 (see methods). Data are from two biological replicates.

G Scatter plots show the comparisons of whole-genome bisulfite sequencing (WGBS) data between TGFβ + RA + VitC iTregs versus TGFβ iTregs. The differentially methylated CpGs (DM-CpGs) are shown in color, and the numbers are shown on top of each graph.

H–J Box-and-whisker plots of DNA methylation levels for DM-CpGs less methylated in TGFβ + RA + VitC iTregs versus TGFβ iTregs (H), DM-CpGs less methylated in WT Treg cells versus CD4$^+$ naïve T cells (I) and DM-CpGs less methylated in WT Treg cells versus *Tet2/3* DKO Treg cells (J). DM-CpGs denotes the CpGs in the respective cell types used for the comparison. Boxplots show the median and quartiles with the whiskers extending to the most extreme data point within 1.5 times the interquartile range. *P*-values are shown above relevant comparisons and are calculated using an analysis of variances with Tukey's post hoc test. Data are from two biological replicates.

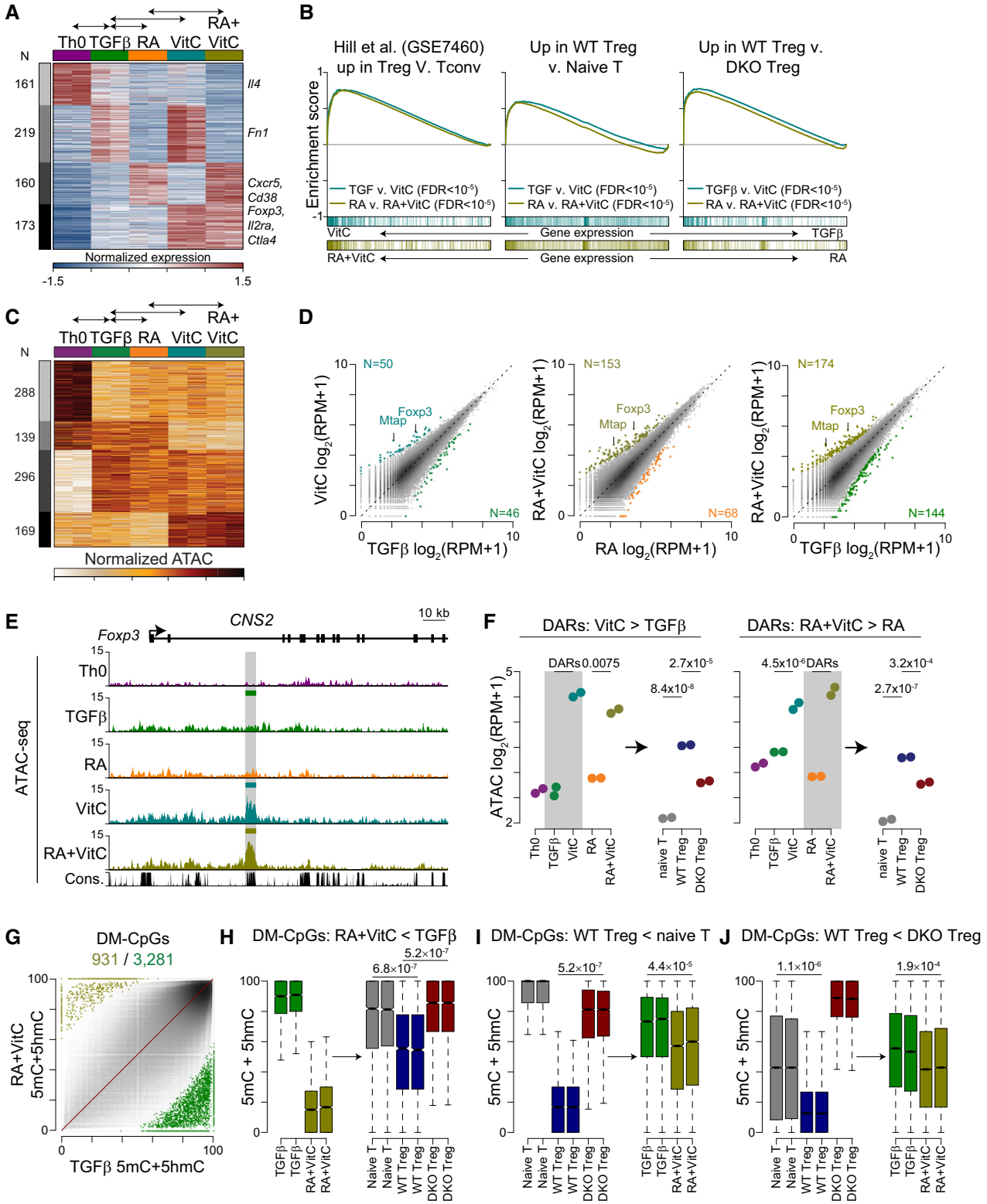

Figure 5.

(Fig 5A, *arrows*, Dataset EV9) identified clusters with distinct gene expression patterns (cluster 1, genes whose expression was largely suppressed in iTreg cells compared with Th0 cells; cluster 2, genes whose expression in iTreg cells was suppressed by RA; cluster 3, genes induced by TGFβ +RA and further induced by VitC; and cluster 4, genes—including the Treg signature genes *Foxp3*, *Nrp1*, *Ikzf4*, *Ccr6*, *Il2ra*, and *Ctla4*, Fig EV2B—that showed the strongest induction of gene expression with VitC in the presence or absence of RA).

Consistent with enrichment of the IL2/STAT5 signaling gene set and depletion of the E2F target gene set in WT compared with *Tet2/3* DKO Treg cells, the IL2/STAT5 signaling gene set was induced while the E2F target gene set was depleted by vitamin C treatment (GSEA, Fig EV2C). Genes upregulated (i) in WT Treg cells compared either with conventional $CD4^+$ T cells (Hill *et al*, 2007) or with $CD4^+$ naïve T cells (our data) and (ii) in WT Treg cells compared with *Tet2/3* DKO Treg cells (our data) were highly represented in iTreg cells differentiated with TGFβ + VitC or TGFβ +RA + VitC, compared with cells differentiated with TGFβ alone or TGFβ + RA (GSEA, Fig 5B). Conversely, genes downregulated in WT Treg cells compared either with conventional $CD4^+$ T cells (Hill *et al*, 2007) or with $CD4^+$ naïve T cells and genes downregulated in WT Treg cells compared with *Tet2/3* DKO Treg cells were underrepresented in iTregs generated with TGFβ + VitC or TGFβ + RA + VitC compared with iTregs differentiated with TGFβ alone or TGFβ + RA (GSEA, Fig EV2D). Thus, vitamin C acts via TET proteins to promote the transcription of Treg signature genes during iTreg differentiation *in vitro*.

In parallel, we analyzed the chromatin accessibility changes in these cell types by ATAC-seq. K-means clustering of the 892 regions differentially accessible in selected pairwise comparisons (Fig 5C, *arrows*, Dataset EV10) in Th0 and iTreg cells identified clusters with distinct patterns of chromatin accessibility changes: regions that lost chromatin accessibility in all iTreg cells compared with Th0 cells (cluster 1); regions that lost accessibility in iTreg cells differentiated in the presence of vitamin C compared with Th0 cells or to iTreg cells differentiated in the absence of vitamin C (cluster 2); regions that were more accessible in iTreg compared with Th0 cells (cluster 3); and regions that were most accessible in iTreg cells differentiated in the presence of vitamin C (cluster 4) (Fig 5C). Vitamin C increased the number of differentially accessible regions in all pairwise comparisons (Fig 5D), but RA had minimal effects (Fig EV2E). The conserved non-coding sequence *CNS2* was the major region in the *Foxp3* locus whose accessibility was increased by treatment with vitamin C; it was barely accessible, if at all, in Th0 cells or in TGFβ or TGFβ + RA iTregs (Fig 5E). Differentially accessible regions (DARs) that were more accessible in iTregs generated with TGFβ + VitC compared with TGFβ alone (Fig 5F, *left*), or in TGFβ + RA + VitC iTregs compared with TGFβ + RA iTregs (Fig 5F, *right*), were also more accessible in endogenous WT Treg cells compared with either $CD4^+$ naïve T cells or endogenous Treg cells isolated from *Tet2/3* DKO mice. Overall, vitamin C not only skewed the gene expression profiles of iTreg cells toward those of endogenous Treg cells, but also enhanced the chromatin accessibility changes occurring during iTreg differentiation *in vitro*, to resemble the changes induced by TET enzymes during endogenous Treg differentiation *in vivo*.

As in all proliferating immune cell types that we have examined —Th1 and Th2 cells, iTreg cells, and B cells (Tsagaratou *et al*, 2014; Yue *et al*, 2016; Lio *et al*, 2019a)—iTreg cells activated and differentiated with TGFβ alone showed a sharp decrease in 5hmC levels by 3 days and a further drop by 6 days of differentiation (Fig EV2F). In both cases, this drop was partially prevented by the addition of vitamin C. In line with this, nearly all of DhmRs (99.9%) were more hydroxymethylated in TGFβ + RA + VitC iTregs compared with iTregs generated with TGFβ alone (Fig EV2G, Dataset EV11). As examples, genome browser tracks and quantified 5hmC signal for the *Foxp3* and *Il2ra* genes are shown in Fig EV2H and I; again, 5hmC levels in the latter part of gene bodies correlated well with the levels of gene expression (Fig EV2J). Overall, we conclude that despite the strong global decrease in 5hmC in T cells activated *in vitro*, addition of vitamin C during TGFβ-induced iTreg differentiation substantially increased genome-wide 5hmC levels.

WGBS analysis of DNA methylation patterns showed that 4,212 CpGs were differentially methylated between iTreg cells differentiated with TGFβ alone and iTreg cells generated with TGFβ + RA + VitC (Dataset EV12); cells differentiated with TGFβ alone contained more highly methylated DM-CpGs (3,281) than TGFβ + RA + VitC iTreg cells (931, Fig 5G). DM-CpGs demethylated in iTreg cells generated with TGFβ + RA + VitC versus TGFβ alone (Fig 5H, *left*) were also demethylated in endogenous WT Treg cells, compared with either naïve T cells or endogenous Treg cells from *Tet2/3* DKO mice (Fig 5H, *right*). Similarly, DM-CpGs that were demethylated in WT Treg cells compared with either naïve T cells or *Tet2/3* DKO Treg cells (Fig 5I and J, *left*) were also demethylated in iTreg cells generated with TGFβ + RA + VitC compared with TGFβ alone (Fig 5 I and J, *right*). In contrast, DM-CpGs that were more methylated in TGFβ + RA + VitC versus TGFβ alone iTreg cells showed no difference in methylation levels when naïve T cells, WT Treg cells, and *Tet2/3* DKO Treg cells were compared (Fig EV2K); and DM-CpGs that were more methylated in WT Tregs compared with naïve T cells or *Tet2/3* DKO Treg cells displayed similar methylation levels in iTreg cells generated with TGFβ + RA + VitC compared with TGFβ alone (Fig EV2L and M). Together these data emphasize the clear correspondence between TET-dependent genome-wide demethylation of endogenous Tregs *in vivo*, and vitamin C-dependent genome-wide demethylation of iTregs induced with TGFβ + RA *in vitro*.

Overall, our data demonstrate that vitamin C potentiates Treg signatures during iTreg differentiation *in vitro* at the transcriptional, chromatin accessibility, 5hmC distribution, and DNA methylation levels.

Increased chromatin accessibility correlates with increased 5hmC and decreased DNA methylation

We examined the relation between 5hmC levels and DNA methylation status in differentially accessible regions (DARs) identified by ATAC-seq (Fig 6). The 2,270 regions with higher accessibility in WT Treg cells compared with *Tet2/3* DKO Treg cells showed more 5hmC deposition at the center of the accessible regions in WT Treg cells; correspondingly, DNA methylation (5mC + 5hmC) was lower in WT compared with *Tet2/3* DKO Treg cells in the 11,303 CpGs covered by these DARs (Fig 6A, *top*). In contrast, the 1,201 regions with decreased accessibility in WT Treg cells compared with *Tet2/3* DKO Treg cells were depleted of 5hmC in WT Treg cells, and the 4,785 CpGs covered by these DARs showed less pronounced DNA demethylation in WT Treg compared with *Tet2/3* DKO Treg cells (Fig 6A, *bottom*). Moreover, regions located ±1kb of DM-CpGs that were demethylated in WT Tregs compared with either naïve T cells or *Tet2/3* DKO Tregs (Appendix Fig S6A) were also considerably more accessible in WT Tregs compared with naïve T cells or *Tet2/3* DKO Tregs (Appendix Fig S6B).

Similarly, the 174 regions with increased accessibility in iTregs differentiated with TGFβ + RA + VitC had increased 5hmC and decreased DNA methylation compared with the same regions in iTregs differentiated with TGFβ alone (Fig 6B, *top*). In contrast, the

144 regions with decreased accessibility in the same comparison showed only a minor increase in 5hmC and no changes in DNA methylation (Fig 6B, *bottom*). These findings are consistent with our previous data in NKT cells, pro-B cells, and mature B cells (Lio *et al*, 2016; Tsagaratou *et al*, 2017a; Lio *et al*, 2019a). The lower magnitude of the change observed in iTregs differentiated *in vitro*

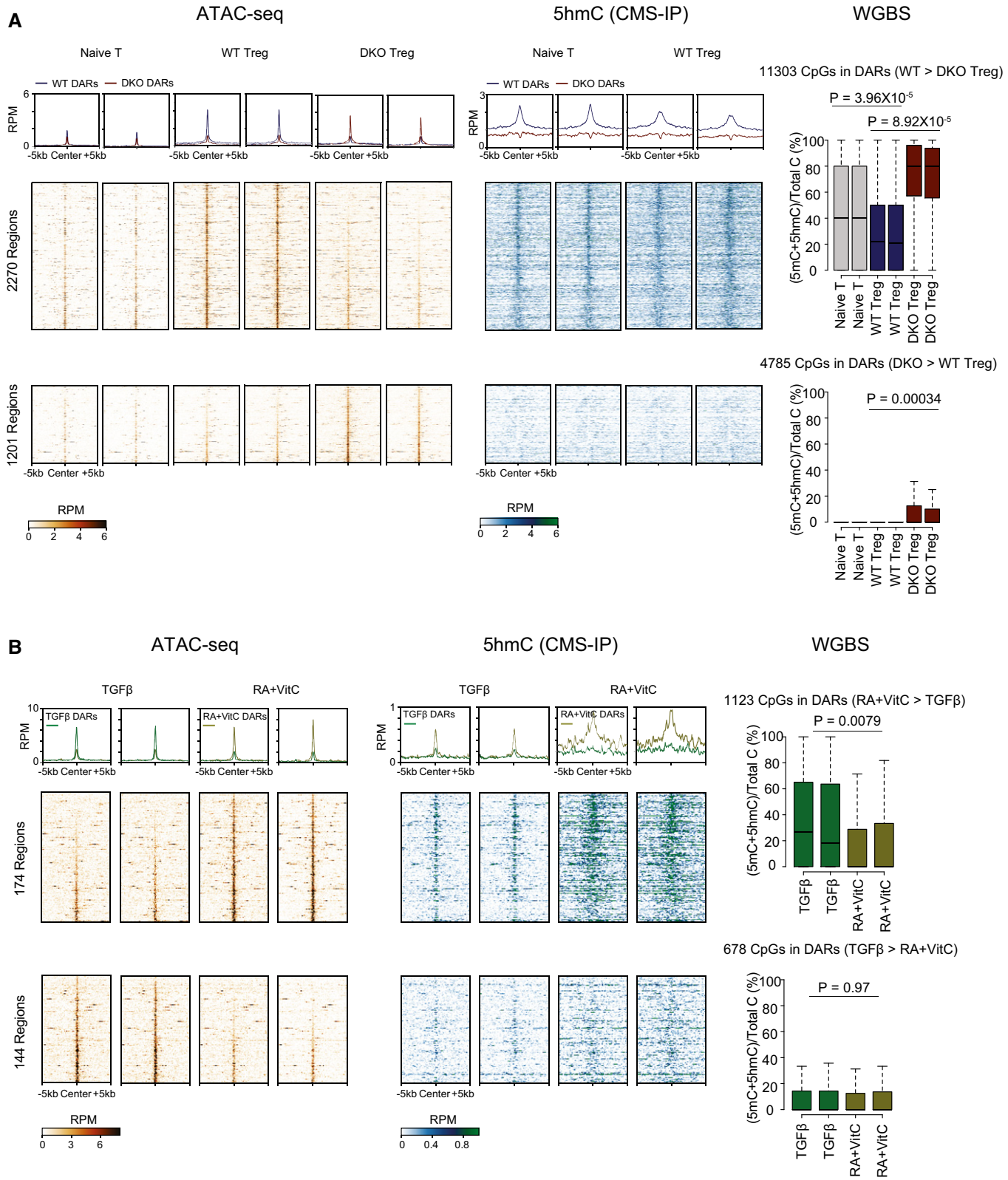

Figure 6.

Figure 6. Correlations among chromatin accessibility, 5hmC distribution, and DNA methylation status.

A *Left*: differentially accessible regions (DARs) between WT Treg cells and *Tet2/3* DKO Treg cells. 2,270 regions are more accessible in WT Treg cells (*upper panel*); 1,201 regions are less accessible in WT Treg cells (*lower panel*). *Middle:* 5hmC distribution assessed by CMS-IP in the DARs shown on the left. *Right:* DNA methylation status assessed by WGBS in DARs shown on the left: 11,303 CpGs in 2,270 regions more accessible in WT Treg cells (*upper panel*); 4,785 CpGs in 1,201 regions less accessible in WT Treg cells (*lower panel*). $CD4^+$ naïve T cells were used as a reference. *P*-values are calculated using analysis of variance and boxplots show the median and quartiles with the whiskers extending to the most extreme data point within 1.5 times the interquartile range.

B *Left*: differentially accessible regions (DARs) between TGFβ iTregs and TGFβ + RA + VitC iTregs. 174 regions are more accessible in TGFβ + RA + VitC iTregs (*upper panel*); 144 regions are less accessible in TGFβ + RA + VitC iTregs (*lower panel*). *Middle:* 5hmC distribution assessed by CMS-IP in the DARs shown on the left. *Right*: DNA methylation status assessed by WGBS in DARs shown on the left: 1,123 CpGs in 174 regions more accessible in TGFβ + RA + VitC iTregs (*upper panel*); 678 CpGs in 144 regions less accessible in TGFβ + RA + VitC iTregs (*lower panel*). *P*-values are calculated using analysis of variance and boxplots show the median and quartiles with the whiskers extending to the most extreme data point within 1.5 times the interquartile range.

likely reflects the sharp decrease in 5hmC levels in T cells upon activation and/or differentiation in cell culture.

Taken together, there is a strong positive correlation of increased 5hmC levels and decreased DNA methylation with increased chromatin accessibility in WT Tregs versus *Tet2/3* DKO Tregs *in vivo* and in iTregs differentiated with TGFβ + RA + VitC versus TGFβ *in vitro*.

Enrichment of STAT motifs and increased STAT5 occupancy in accessible regions of vitamin C-treated iTreg cells

We used de novo and known motif enrichment analyses to ask whether vitamin C preferentially increased the genome-wide occupancy of specific transcription factors in iTreg cells. Comparing three sets of differentially accessible regions (DARs) induced by vitamin C, we observed a striking enrichment for consensus binding sequences (TTCnnnGAA) for STAT transcription factors in DARs that were more accessible in TGFβ + RA + VitC versus TGFβ iTregs; TGFβ + VitC versus TGFβ iTregs; and TGFβ + RA + VitC versus TGFβ + RA iTregs (Figs 7A and EV3A). The key Treg cytokine IL-2, known to be essential for Treg differentiation *in vivo*, is typically added at high concentrations (100 U/ml) to cell culture media during iTreg differentiation *in vitro*, and induces STAT5 phosphorylation and activation through JAK-STAT pathway activation (Abbas *et al*, 2018; Ross & Cantrell, 2018). We therefore examined the features of iTreg differentiation in response to varying IL-2 concentrations in the presence or absence of RA and vitamin C (Figs 7B and EV3B and C). We labeled naïve $CD4^+$ T cells from Foxp3-IRES-eGFP reporter mice with Cell Trace Violet (CTV), a dye that is diluted by half with each cell division; differentiated them into iTregs in media containing TGFβ or TGFβ + RA + VitC with varying amounts of IL-2 (0, 1, 5, 10, 25, 50, 75, and 100 U/ml); and monitored the percentage of Foxp3 (eGFP)-expressing cells, cell proliferation, and cell survival on a daily basis. iTregs differentiated with TGFβ + RA + VitC showed a striking increase in the level and stability of Foxp3 expression, compared with iTregs differentiating in the presence of TGFβ alone (Figs 7B and EV3B). On day 2 of differentiation, over 80% of cells activated and cultured in TGFβ + RA + VitC media expressed Foxp3, compared with only ~40% of cells activated and cultured in media containing TGFβ alone (Fig EV3B). The increased Foxp3 stability was apparent in TGFβ + RA + VitC iTregs compared with TGFβ iTregs as a function of the number of days of differentiation as well as the number of cell divisions, and was observed in both the absence and presence (100 U/ml) of IL-2 (Fig 7B and C). Notably, during the first 5 days of differentiation, the presence or absence of IL2 in culture media had no effect on cell proliferation as assessed by CTV dilution (Fig 7B) or the percentage of Foxp3-expressing cells (Fig EV3B), likely because of endogenous IL2 secretion by the activated $CD4^+$ T cells. The decrease in the percentage of Foxp3-expressing cells at high levels of IL-2 (Fig EV3B) is consistent with the higher rates of cell proliferation under these conditions. Thus, as previously noted (Yue *et al*, 2016), vitamin C is a major regulator of Foxp3 levels and stability in differentiating iTregs.

The addition of RA and vitamin C also led to a moderate increase in cell viability (Figs 7D and EV3C and D). Starting on day 6, the percentage of viable iTreg cells correlated with the amount of IL-2 in culture for both TGFβ alone and TGFβ + RA + VitC conditions: In particular, survival at low IL-2 concentrations (1 and 5 U/ml) was enhanced in the presence of RA and VitC (Figs 7D and EV3C and D). In addition, iTregs differentiated with TGFβ + RA + VitC showed increased phospho-STAT5 levels compared with iTregs differentiated with TGFβ alone; the increase was most obvious at low levels of IL-2 (3–10 U/ml) and was observed in iTreg cells differentiated in the presence of either 0 or 100 U/ml IL-2 (Figs 8A and B, and EV4A and B). Consistent with this increase, we also observed increased binding of STAT5 to the *Foxp3 CNS2* enhancer and to a known STAT5-binding region in an intronic region of the *Il2ra* gene

Figure 7. Enrichment of STAT motifs in regions that are more accessible with vitamin C treatment.

A Scatter plot of pairwise comparison of chromatin accessibility changes between TGFβ + RA + VitC versus TGFβ iTregs showing the top identified motifs.

B $CD4^+$ naïve T cells were sorted from Foxp3-IRES-eGFP reporter mice, labeled with cell proliferation dye cell trace violet, and differentiated into iTreg cells with TGFβ alone or TGFβ + RA + VitC with different amounts of IL-2. Cells in the cultures were analyzed daily by flow cytometry. The two upper panels show representative dot plots of Foxp3 expression versus cell proliferation for TGFβ alone and TGFβ + RA + VitC iTregs with 100 U/ml IL-2 from day 2 to day 9. The two lower panels show representative dot plots of Foxp3 expression versus cell proliferation for TGFβ alone and TGFβ + RA + VitC iTregs with 0 U/ml IL-2 from day 2 to day 9.

C Graph showing the percentage of $Foxp3^+$ cells at each day for TGFβ iTregs and TGFβ + RA + VitC iTregs with either 0 U/ml IL-2 or 100 U/ml IL-2. Error bars show mean ± SD from three biological replicates.

D Graphs depicting the percentage of viable cells for TGFβ iTregs (*left*) and TGFβ+RA+VitC iTregs (*right*) differentiated with 0, 1, 5, and 10 U/ml IL-2. Error bars show mean ± SD from three biological replicates.

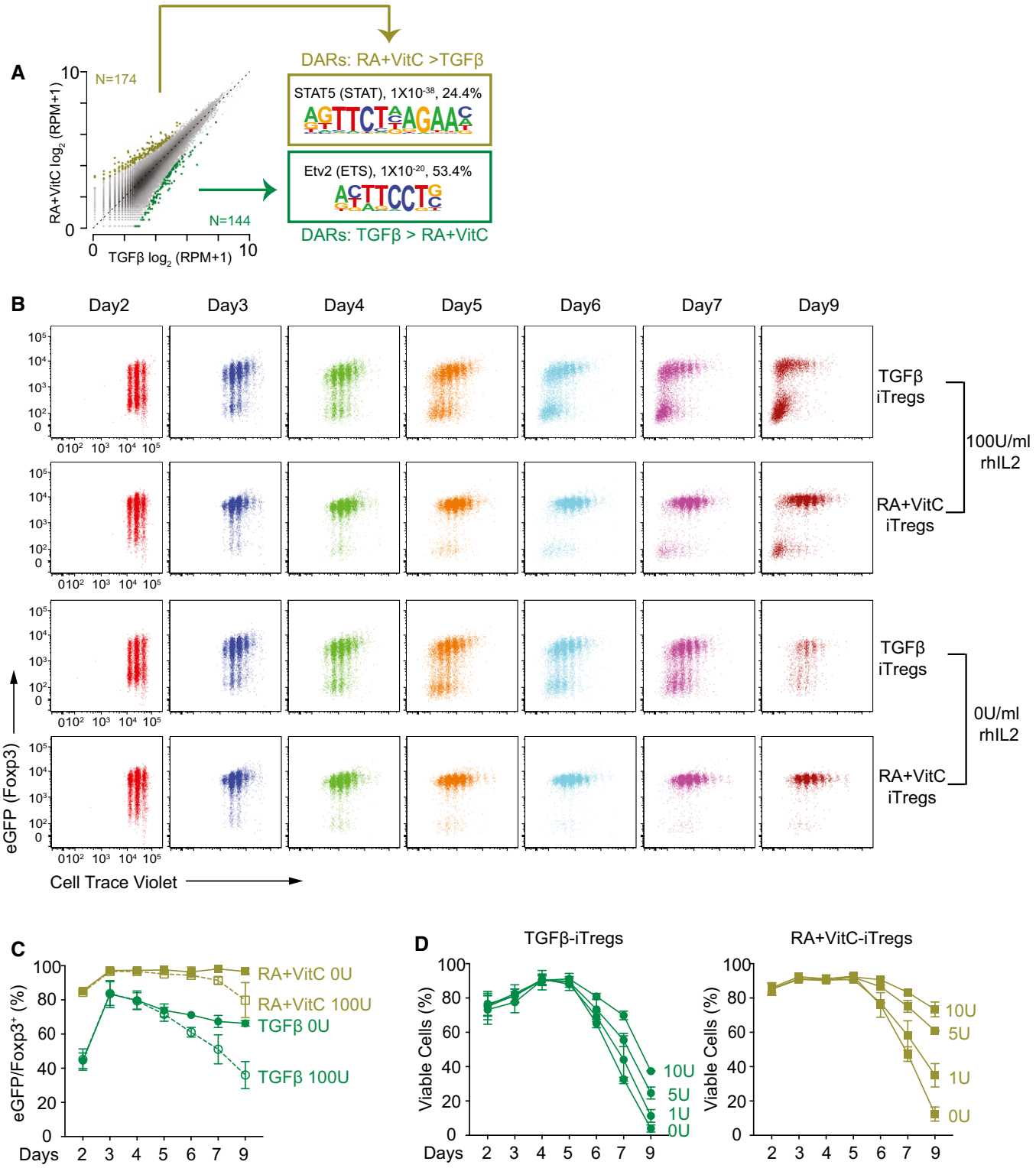

Figure 7.

(Li *et al*, 2017) (Fig 8C). Concomitantly, on day 6 after differentiation with 100 U/ml IL-2, we observed an increase in the expression of *Il2ra* mRNA by RNA-seq in iTregs differentiated with TGFβ + RA + VitC compared with iTregs differentiated with TGFβ alone (Fig EV4C, *left panel*), as well as increased expression of IL2Rα (CD25) protein by flow cytometry on day 6 after differentiation with either 0 or 100 U/ml IL-2 (Figs 8D and E, and EV4D and E). The effect on *Il2rb* mRNA and IL2Rβ (CD122) protein was less pronounced (Fig EV4C and F), while expression of *Il2rg* chain mRNA and the common gamma chain (γc) protein decreased after

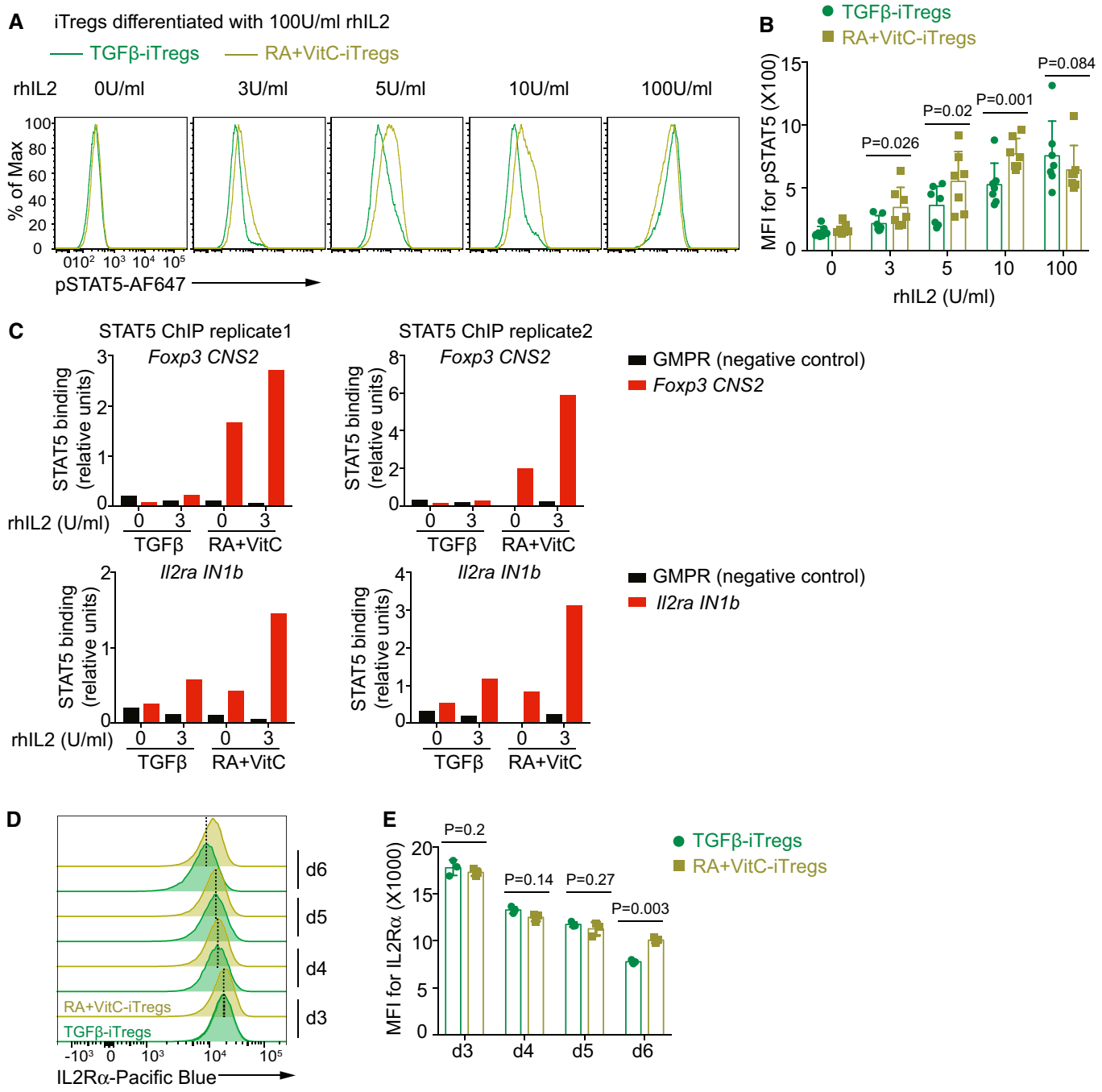

Figure 8. Vitamin C facilitates the binding of STAT5 and maintains IL2Rα expression in iTregs.

A, B CD4$^+$ naïve T cells were sorted from Foxp3-IRES-eGFP reporter mice and differentiated into iTreg cells with TGFβ alone or TGFβ + RA + VitC in the presence of 100 U/ml IL-2 in cultures. On day 6, cells were restimulated without IL-2 or with 3, 5, 10, and 100 U/ml IL-2 at 37°C for 1hr, and stained for phospho-STAT5. Representative histogram overlay of phospho-STAT5 staining for TGFβ and TGFβ + RA + VitC iTregs after IL-2 restimulation (A). Graph depicting the geometric mean fluorescent intensity (MFI) of phospho-STAT5 in TGFβ and TGFβ + RA + VitC iTregs after IL-2 restimulation; each dot represents cells from an individual mouse (B). Data are from seven biological replicates. *P*-values are calculated using two-tailed paired Student's *t*-test, and error bars show mean ± SD.

C ChIP-qPCR showing STAT5 occupancy at *Foxp3 CNS2* and *IL2Rα IN1b* regions in TGFβ and TGFβ + RA + VitC iTregs without or with 3 U/ml IL-2 restimulation. GMPR is a negative control region. Data are from two biological replicates.

D, E Representative histogram overlay (D) and geometric MFI (E) of IL2Rα staining for TGFβ and TGFβ + RA + VitC iTregs on day 3 to day 6 after differentiation in the presence of 100 U/ml IL-2. Data are from three biological replicates. *P*-values are calculated using two-tailed paired Student's *t*-test, and error bars show mean ± SD.

differentiation (Fig EV4C and G). We observed similar effects when iTreg cells were differentiated in the absence of RA. Compared with iTregs differentiated with TGFβ alone, iTreg cells differentiated with TGFβ + VitC showed an increased expression of both *Il2ra* mRNA by RNA-seq (Fig EV5A) and IL2Rα (CD25) protein by flow cytometry (Fig EV5B). iTregs differentiated with TGFβ + VitC also showed increased phospho-STAT5 levels especially at low level of IL-2 (10 U/ml) (Fig EV5C).

Overall, these data show that the presence of RA and vitamin C during iTreg differentiation sensitizes the response to IL-2, by increasing both STAT5 phosphorylation and STAT5 occupancy of two key enhancers in the *Foxp3* and *Il2ra* loci, and also by maintaining the levels of IL2Rα in response to limiting IL-2 stimulation.

Discussion

We showed previously that the two TET enzymes present at highest levels in mouse Treg cells, Tet2 and Tet3, control DNA demethylation of the *Foxp3 CNS2* enhancer and the stability of Foxp3 expression. To demonstrate these points, we used TET loss-of-function in endogenous Treg cells and TET gain-of-activity in TET activator vitamin C-treated iTreg cells *in vitro*. Vitamin C functions through TET proteins to mediate *CNS2* demethylation and increase in Foxp3 MFI, as these effects are abolished in TET-deficient iTreg cells treated with vitamin C ((Yue *et al*, 2016), Appendix Fig S5). In this study, we have extended these results to a genome-wide level, by investigating for the first time the transcriptional profiles, chromatin accessibility landscapes, and DNA methylation/ hydroxymethylation changes in endogenous WT and TET-deficient Treg cells and in TGFβ-induced iTreg cells after the addition of vitamin C. We show that TET enzymes promote the acquisition of the molecular programs of gene expression, chromatin accessibility, and DNA methylation that are characteristic of Treg cells *in vivo*; moreover, treatment of differentiating iTreg cells with the TET activator vitamin C *in vitro* mimics these effects, albeit to a lesser extent.

Motif enrichment analysis of differentially accessible and differentially hydroxymethylated regions pointed to a correlation between Treg-specific and TET-regulated epigenetic alterations, identified by comparing WT $CD4^+$ naïve T versus WT Treg cells and WT Treg versus *Tet2/3* DKO Treg cells, respectively. Consensus binding sequences of bZIP, RHD and NR transcription factor families were enriched in differentially accessible regions located in Treg-specific/TET-regulated cluster (cluster 2 in Fig 4C and D) and in Treg-specific DhmRs (Fig EV1C). The DNA methylation levels surrounding consensus binding motifs of these transcription factor families were also Treg-specific and TET-regulated. Specific members of each of these transcription factor families are known essential regulators of Treg development and function. The consensus binding motifs for most of these transcription factors typically do not contain CpGs (Fig 3D), implying that direct modulation of transcription factor binding by TET-dependent demethylation of the binding site is not likely to be a widespread mechanism for TET-dependent regulation of gene expression. It is more likely that the relevant transcription factors recruit Tet2 and Tet3 proteins to promoters and enhancers to maintain their chromatin accessibility and demethylated status (Wang *et al*, 2015; Lio *et al*, 2016; Suzuki *et al*, 2017; Sardina *et al*, 2018; Lio *et al*, 2019a).

Our data also reveal an intriguing connection between TET activity, vitamin C, and responses to IL-2, a key cytokine critical for Treg development, differentiation, and function (Abbas *et al*, 2018; Ross & Cantrell, 2018). IL-2 is well established as essential for Treg function: mice with germline deletion of *IL2*, *IL2ra*, and *IL2rb* develop severe autoimmune diseases (Fontenot *et al*, 2005) and mice with Treg-specific ablation of *IL2ra* and *IL2rb* exhibit more severe lethal autoimmunity than mice with germline deletion of the same genes, exhibiting phenotypes similar to those of *Foxp3*-deficient *scurfy* mice (Chinen *et al*, 2016; Toomer *et al*, 2019). Likewise, *STAT5a/b*-deficient mice fail to generate Treg cells and also develop fatal autoimmunity (Snow *et al*, 2003). Thus, the IL2-IL2R-STAT5 signaling axis is essential for the functional programming of Treg cells and maintenance of immune homeostasis (Ross & Cantrell, 2018). We observed that TET deletion *in vivo* resulted in impaired IL2/STAT5 signaling, with the IL2/STAT5 gene set being underrepresented in *Tet2/3* DKO Treg cells compared with WT Treg cells. Conversely, we found that STAT motifs were enriched in differentially accessible regions induced by vitamin C and that iTregs induced in the combined presence of TGFβ, RA, and vitamin C survived better in low IL-2 media and were more responsive to stimulation with low IL-2 concentrations than iTregs induced in the presence of TGFβ alone. This feature was associated with increased levels of phospho-STAT5, increased occupancy of STAT5 at key *Foxp3* and *Il2ra* enhancers and increased IL2Rα mRNA and protein levels (Fig 8).

Treg cells lacking a single genomic region, *Foxp3 CNS2*, show cell cycle-dependent loss of Foxp3 upon *in vitro* stimulation through the TCR (Feng *et al*, 2014b; Li *et al*, 2014). Notably, this effect can be rescued by culturing the *CNS2*-deficient Treg cells in the presence of high concentrations of IL-2 (Feng *et al*, 2014b). Thus, the CpG-rich intronic enhancer, *Foxp3 CNS2*, functions as a sensor of the cytokine IL-2 and its downstream target STAT5 to prevent cell cycle-dependent loss of Foxp3 expression in Treg cells *in vivo (*Feng *et al*, 2014b*)*. Here, we show that *CNS2* is also a very specific sensor of TET activity and the TET activator vitamin C during *in vitro* iTreg differentiation, based on vitamin C-induced, TET-dependent, and Treg-specific demethylation patterns, vitamin C-induced and Treg-specific chromatin accessibility landscapes, and vitamin C-induced STAT5 occupancy at low IL-2 concentrations (*CNS2* contains several STAT5-binding motifs).

TET proteins are increasingly recognized to be responsive to metabolic influences including those arising from diet and nutrition, and TET and vitamin C deficiencies are both well established as a risk factor for blood cancers (Loria *et al*, 2000; Khaw *et al*, 2001; Huijskens *et al*, 2016; Lio *et al*, 2019b). Our data emphasize that, in addition, low plasma vitamin C levels may also predispose individuals to autoimmune disease secondary to decreased function of both thymically derived and peripherally generated Tregs. Vitamin C deficiency is expected to reduce the function of all Fe (II) and 2-oxoglutarate-dependent dioxygenases including TET enzymes, and to result in suboptimal function of both thymically derived and peripherally generated Tregs. It would be interesting to conduct an epidemiological study of the relation between plasma vitamin C levels and autoimmune disease in humans, similar to previous studies relating plasma vitamin C levels to overall mortality and cancer (Loria *et al*, 2000; Khaw *et al*, 2001; Huijskens *et al*, 2016).

Materials and Methods

Mice

Foxp3-eGFP reporter mice (strain 006769) were originally obtained from Jackson Laboratory and further backcrossed to B6/C57 background for more than 10 generations. *Tet2*$^{fl/fl}$*Tet3*$^{fl/fl}$ Foxp3-eGFP mice and *Tet2*$^{fl/fl}$*Tet3*$^{fl/fl}$ Foxp3-eGFP CD4Cre mice were generated in our laboratory using B6/Taconic background "Artemis" ES cells. All mice were on the B6 background and maintained in a specific pathogen-free animal facility in the La Jolla Institute for Immunology. Age and sex of the mice used for each experiment were stated in the methods. Deletion of *Tet2* and *Tet3* was mediated by CD4Cre, therefore in order to minimize the potential cell-extrinsic effects on Treg cells in this animal model, we used young (3-week-old) mice for all the genomic studies. All animal procedures were reviewed and approved by the Institutional Animal Care and Use Committee of the La Jolla Institute for Immunology and were conducted in accordance with institutional guidelines.

RNA-seq library preparation

For WT and *Tet2/3* DKO Treg samples, CD4$^+$eGFP$^+$ Treg cells were sorted from 3-week-old *Tet2*$^{fl/fl}$*Tet3*$^{fl/fl}$ Foxp3-eGFP CD4CRE mice and *Tet2*$^{fl/fl}$*Tet3*$^{fl/fl}$ Foxp3-eGFP littermate control mice (males). For Th0 cells and iTreg cells, CD4$^+$eGFP$^-$CD25$^-$CD62L^{hi}CD44^{lo} naïve T cells were sorted from Foxp3-eGFP reporter mice (5–6 weeks old, female) and differentiated into Th0 cells (activated with anti-CD3 and anti-CD28 antibodies in the absence of polarizing cytokines or neutralizing anti-cytokine antibodies) and iTreg cells under four different conditions: TGFβ alone; TGFβ + vitamin C (VitC); TGFβ + retinoic acid (RA); TGFβ + RA + VitC. eGFP$^-$ Th0 cells and eGFP$^+$ iTreg cells were sorted on day 6 after differentiation.

Total RNA was isolated from samples using RNeasy plus mini or micro kit (Qiagen). RNA-sequencing libraries were prepared using Truseq stranded mRNA kit (Illumina) according to the manufacture's protocol. Libraries were pooled in equal quantity and sequenced using Illumina HiSeq 2500 (Illumina) as 50-base-pair paired end reads (for WT and *Tet2/3* DKO Treg samples) and 125-base-pair paired end reads (for Th0 and iTreg samples).

RNA-seq analysis

Processing of RNA-seq data was performed similar to that previously described (Barwick *et al*, 2016). Specifically, RNA-seq FASTQ files were quality and adapter trimmed using Trim Galore (v0.4.2) prior to mapping to the UCSC mouse genome mm9 using STAR (v2.5.3a) (Dobin *et al*, 2013) with the following parameters "-quantMode GeneCounts --chimSegmentMin 20 --outSAMtype BAM Unsorted" and the UCSC mm9 KnownGenes gtf transcript file. BAM files from STAR were sorted and duplicates were marked Samtools (v1.7) (Li *et al*, 2009). Quantification of gene expression used exons defined by the "TxDb. Mmusculus.UCSC.mm9.knownGene" transcript database (v3.2.2) and the summarizeOverlaps function in mode "IntersectionNotEmpty" from the GenomicAlignments package (v1.20.1) (Lawrence *et al*, 2013) in R (v3.6.1) (Gentleman *et al*, 2004). Fragments per kilobase per million reads (FPKM) normalization was performed in R based on the number of exonic mapped reads per gene relative to all mapped autosomal reads. Differentially expressed genes were determined using EdgeR (v3.12.1) (Robinson *et al*, 2010) where a maximum FDR of 0.05 and minimum fold-change of 2 were enforced to determine significance. Differentially expressed genes were organized by K-means clustering using the "kmeans" function of the stats package in R (v3.6.1). Gene Set Enrichment Analysis (GSEA v4.0.2) was performed using a pre-ranked list based on the -$\log_{10}$(P-value) x sign(log fold-change) for each comparison using the mSigDB curated database (v6.2) (Subramanian *et al*, 2005).

ATAC-seq library preparation

For WT and *Tet2/3* DKO Treg samples, CD4$^+$eGFP$^+$ Treg cells were sorted from 3-week-old *Tet2*$^{fl/fl}$*Tet3*$^{fl/fl}$ Foxp3-eGFP CD4CRE mice and *Tet2*$^{fl/fl}$*Tet3*$^{fl/fl}$ Foxp3-eGFP littermate control mice (females). For Th0 cells and iTreg cells, CD4$^+$eGFP$^-$CD25$^-$CD62L^{hi}CD44^{lo} naïve T cells were sorted from Foxp3-eGFP reporter mice (5–6 weeks old, male) and differentiated into Th0 cells and iTreg cells under four different conditions: TGFβ alone; TGFβ + vitamin C (VitC); TGFβ + retinoic acid (RA); and TGFβ + RA + VitC. eGFP$^-$ Th0 cells and eGFP$^+$ iTreg cells were sorted on day 6 after differentiation.

Cells were counted after sorting and 50,000 cells were washed once with 120 μl ice-cold 1× PBS and spin down at 500 *g* for 10 min at 4°C. Cell pellets were resuspended in 50 μl cold lysis buffer (10 mM Tris–HCl pH7.4, 10 mM NaCl, 3 mM $MgCl_2$, 0.1% NP-40) and immediately spin down at 500 *g* for 15 min at 4°C. The supernatant was discarded and the nuclei pellets were resuspended in 25 μl of transposition mix (12.5 μl 2× Nextera Tagment DNA Buffer, 1.25 μl Nextera Tagment DNA Enzyme, 11.25 μl H2O), incubated at 37°C for 30mins. DNA was purified using Zymo DNA Clean and Concentrator Kit (Zymo Research). Samples were then amplified using KAPA HiFi HotStart ReadyMix (KAPA Biosystems) for 11 cycles and purified using Ampure XP Beads (Beckman Coulter). The libraries were sequenced as 50-base-pair paired end reads using Illumina Hiseq 2500 (Illumina).

ATAC-seq analysis

ATAC-seq FASTQ files were quality and adapter trimmed using Trim Galore (v0.4.2) prior to mapping to the UCSC mouse genome mm9 using Bowtie2 (v2.2.6) (Langmead & Salzberg, 2012) with default parameters. Mapped SAM files were converted to BAM, and putative PCR duplicates were marked with Samtools (v1.7) (Li *et al*, 2009). Regions of chromatin accessibility were determined using MACS2 (v2.1.0.20151222) with the following settings "-g mm -q 0.01" (Zhang *et al*, 2008). The union of accessible regions in all samples were determined using the "GenomicRanges" package (v1.36.1) in R, and data were normalized to reads in peaks per million (RPM) as previously described (Barwick *et al*, 2018). Differentially accessible regions were determined using EdgeR (v3.26.6) with a maximum FDR of 0.05 and a minimum fold-change of 2. K-means clustering was performed using the "kmeans" function of the stats package in R (v3.6.1) and plotted using the custom code similar to the heatmap2 function in R. Genome plots were made with custom R code using the "rtracklayer" package (v1.44.4) (Lawrence *et al*, 2009). ATAC-seq data for Naïve CD4 T cells made

use of ImmGen samples GSM2692322 and GSM2692323, which were used for comparison but not included in differential analyses. Transcription factor motifs were determined using the scanMotifGenomeWide.pl script of HOMER software (Heinz *et al*, 2010), and motifs enriched in differentially accessible regions were determined by Fisher's exact test with FDR correction.

CMS-IP library preparation

$CD4^+eGFP^+CD25^+$ WT Treg cells and $CD4^+eGFP^-CD25^-CD62L^{hi}CD44^{lo}$ naïve T cells were sorted from Foxp3-eGFP reporter mice (5–6 weeks old, male). For iTreg cells, $CD4^+eGFP^-CD25^-CD62L^{hi}CD44^{lo}$ naïve T cells were sorted from Foxp3-eGFP reporter mice (5–6 weeks old, male) and differentiated into iTreg cells under TGFβ alone and TGFβ + RA + VitC conditions. $eGFP^+$ iTreg cells were sorted on day 6 after differentiation.

Sodium bisulfite treatment converts 5hmC into CMS (cytosine-5-methylenesulfonate), which is then recognized by anti-CMS serum with high sensitivity and selectivity (Pastor *et al*, 2011). CMS-IP was performed as previously described (Huang *et al*, 2012). Briefly, genomic DNA was sheared using Covaris S2 and was spiked with two 210-base-pair PCR amplicons (C amplicon and 5hmC amplicon) at a ratio of around 1:20,000. DNA was purified with Ampure XP beads (Beckman Coulter) and processed with NEBNext End Repair and dA-Tailing Modules (NEB), and ligated to methylated Illumina Adaptors using NEBNext Quick Ligation Module (NEB). DNA with ligated adaptors was then treated with sodium bisulfite (MethylCode, Thermo Fisher Scientific) for 4 h, denatured, and immunoprecipitated with anti-CMS serum (input samples were reserved as 1% of total DNA before immunoprecipitation). Samples for immunoprecipitated DNA and input DNA were then purified using Phenol/Chloroform and amplified with index primers using KAPA HiFi HotStart Uracil+ Ready Mix (KAPA Biosystems). The samples after PCR amplification were then purified using Ampure XP Beads (Beckman Coulter) and sequenced as 50- or 100-base-pair paired end reads using Illumina Hiseq 2500 (Illumina).

The spike-in amplicons were generated using lambda phage DNA as template and with dNTP mix or 5-Hydroxymethylcytosine dNTP mix (Zymo Research), respectively. Therefore, the cytosines in the C amplicon were unmethylated (used to monitor the bisulfite conversion efficiency), while the cytosines in the 5hmC amplicon were 5-hydroxymethylated (used for normalization of the number of reads to the global content of 5hmC levels in different samples). Reads that mapped to the 5hmC spike-in control in the CMS-IP samples reflected the global content of 5hmC in each sample: For example, iTreg cells induced with TGFβ had the lowest level of 5hmC assessed by CMS dot blot; thus, the DNA samples from these cells had the largest number of reads that mapped to the spike-in control.

CMS-IP analysis

CMS-IP FASTQ files were quality and adapter trimmed using Trim Galore (v0.4.2). Trimmed FASTQ files were mapped to the *in silico* bisulfite converted mm9 genome with the unmethylated and 5hmC amplicons added as artificial chromosomes. Mapped SAM files were converted to BAM, and putative PCR duplicates were marked with Samtools (v1.7) (Li *et al*, 2009). Normalization was performed using the 5hmC spike-ins. Specifically, the proportion (P_s) of 5hmC spike-in reads to non-duplicate autosomal reads were determined for each sample (S)as follows:

$$P_s = \frac{5hmc\ spikein\ reads}{autosomal\ reads}$$

This proportion of 5hmC spike-in reads was used to create a 5hmC normalization ratio for CMS-IP and input samples separately (Ns), using the following formula:

$$N_s = \frac{\overline{P}}{P_s}$$

where $\overline{P}$ represents the average proportion of 5hmC reads of all CMS-IP or all input samples. A final 5hmC normalization ratio (N_f) was calculated by correcting the 5hmC normalization ratio of CMS-IP samples (N_c) by the 5hmC normalization ratio for their respective input samples (N_i) as follows:

$$N_f = \frac{N_c}{N_i}$$

Subsequently, CMS-IP reads were normalized for reads per million multiplied by the final 5hmC normalization ratio (N_f). A normalization ratio of 1 was used for input samples. The resultant normalization reflected the global content of 5hmC in each sample. Regions of enriched 5hmC were determined using MACS2 (v2.1.0.20151222) with the following settings "-g mm --broad -q 0.01" (Zhang *et al*, 2008). The union of 5hmC enriched regions were determined using the "GenomicRanges" package (v1.36.1) in R, and differentially accessible regions were determined using EdgeR (v3.26.6) with an FDR $\leq$ 0.05 and a fold-change $\geq$ 2.

WGBS library preparation

For WT Treg and $CD4^+$ naïve T-cell samples, $CD4^+eGFP^+CD25^+$ Treg cells and $CD4^+eGFP^-CD25^-CD62L^{hi}CD44^{lo}$ naïve T cells were sorted from Foxp3-eGFP reporter mice (5–6 weeks old, male). For *Tet2/3* DKO Treg sample, $CD4^+eGFP^+CD25^+$ Treg cells were sorted from $Tet2^{fl/fl}Tet3^{fl/fl}$ Foxp3-eGFP CD4CRE mice (3-weeks old, male). For iTreg cells, $CD4^+eGFP^-CD25^-CD62L^{hi}CD44^{lo}$ naïve T cells were sorted from Foxp3-eGFP reporter mice (5–6 weeks old, male) and differentiated into iTreg cells under TGFβ alone and TGFβ + RA + VitC conditions. $eGFP^+$ iTreg cells were sorted on day 6 after differentiation.

Genomic DNA was isolated using PureLink Genomic DNA Mini Kit (Thermo Fisher Scientific, K182001) or FlexiGene DNA Kit (Qiagen, 51206). Unmethylated lambda DNA (Promega, D1521) was spiked into the genomic DNA samples at a ratio of 1:200 to monitor the bisulfite conversion efficiency. The samples were then sheared using Covaris S2, purified with Ampure XP beads (Beckman Coulter) and processed with NEBNext End Repair and dA-Tailing Modules (NEB), and ligated to methylated Illumina Adaptors using NEBNext Quick Ligation Module (NEB). DNA with ligated adaptors was then treated with sodium bisulfite (MethylCode, Thermo Fisher Scientific) for 4hrs and amplified with index primers using KAPA HiFi HotStart Uracil+ Ready Mix (KAPA Biosystems). The samples after PCR amplification were then purified using Ampure XP Beads (Beckman Coulter) and sequenced as 125- or 250-base-pair paired end reads using Illumina Hiseq 2500 (Illumina).

WGBS analysis

WGBS FASTQ files were quality and adapter trimmed using Trim Galore (v0.4.2) prior to mapping to the *in silico* bisulfite converted UCSC mouse genome mm9 using Bismark (v0.19.0) (Krueger & Andrews, 2011) to call Hisat2 (v2.1.0). Mapped BAM files were sorted with Samtools (v1.7) (Li *et al*, 2009), and CpG methylation calls were extracted using bespoke code as previously described (Barwick *et al*, 2016). CpG methylation calls were collapsed to one strand and DNA methylation coverage was determined as CpGs with ≥ 5× coverage per group resulting in DNA methylation data at 18,531,012 CpGs with an average coverage of 14.9× per CpG per sample (range 11.7×–17.8×). Differentially methylated loci were determined using DSS (v2.32.0) (Feng *et al*, 2014a) where significance was determined by an FDR ≤ 0.05 and a mean CpG methylation difference of 0.2. K-means clustering was performed in R (v3.6.1), and CpG loci were annotated using GREAT (v4.0.4) (McLean *et al*, 2010).

Transcription factor-binding motif analyses

Enrichment of transcription factor consensus binding motifs was performed as previously described (Barwick *et al*, 2018). Briefly, consensus binding motifs were determined using HOMER software (http://homer.ucsd.edu/homer/; v4.10). Specifically, the "scanMotifGenomeWide.pl" script was used with default parameters to catalogue motifs in the mm9 genome. Enrichment of motifs in DhmRs, DM-CpGs, and DARs relative to assay coverage was determined using Fisher's exact test with a FDR correction.

In vitro iTreg differentiation

$CD4^+CD25^-CD62L^{hi}CD44^{lo}eGFP^-$ naïve T cells were FACS sorted from spleen and lymph nodes of Foxp3-IRES-eGFP reporter mice (6- to 8-week-old) or $Tet2^{fl/fl}Tet3^{fl/fl}$ Foxp3-eGFP CD4Cre mice (2.5- to 3-week-old), and differentiated into iTregs with plate-bound anti-CD3 (clone 2C11) and anti-CD28 (clone 37.51) antibodies at 1 μg/ml in the presence of 2 ng/ml recombinant human TGFβ (PeproTech) and 100 U/ml rhIL-2. For the conditions with retinoic acid (RA, sigma) and/or vitamin C (VitC, sigma), 100 nM of RA, 100 μg/ml of VitC were added into the culture.

For iTreg cell differentiation in the presence of different IL-2 concentration, $CD4^+$ naïve T cells were sorted and labeled with the proliferation dye cell trace violet (Thermo Fisher Scientific) and differentiated into iTreg cells in the presence of TGFβ alone or TGFβ + RA + VitC at different concentration of rhIL-2 (0, 1, 5, 10, 25, 50, 75, and 100 U/ml). The percentage of Foxp3 $(eGFP)^+$ cells, the percentage of viable cells (assessed using eBioscience fixable viability dye eFluor780), and cell proliferation (assessed using the cell proliferation dye cell trace violet) were monitored from day 2 to day 9 after differentiation.

Cell sorting and flow cytometry

Single-cell suspensions were prepared from spleen and lymph nodes for cell sorting. iTreg cells were collected from *in vitro* cultures for staining or cell sorting. The anti-mouse antibodies used for sorting of $CD4^+CD25^-CD62L^{hi}CD44^{lo}eGFP^-$ naïve T cells and $CD4^+$Foxp3 $(eGFP)^+$ or $CD4^+$Foxp3 $(eGFP)^+CD25^+$ Treg cells are as follows (Clone name, conjugated fluorescence, dilution, manufacturer, and catalog number shown in brackets): CD4 (RM4-5, PerCP-Cy5.5, 1:200, BioLegend, #100540); CD25 (PC61, APC, 1:200, BioLegend, #102012); CD62L (MEL-14, BV421, 1:400, BioLegend, #104436); and CD44 (IM7, PE, 1:200, BioLegend, #103008). The gating strategy used for cells sorting was shown in Appendix Fig S7.

For analysis of the expression levels of IL2R subunits from day 3 to day 6 after primary differentiation of iTregs in the presence of TGFβ alone or TGFβ + RA + VitC, single-cell suspensions were stained with anti-mouse antibodies against the following: CD4 (RM4-5, PerCP-Cy5.5, 1:200, Biolegend, #100540); IL2Rα/CD25 (PC61, Pacific Blue, 1:200, Biolegend, #102021); IL2Rβ/CD122 (TM-β1, PE, 1:75, Biolegend, #123209); and IL2Rγ/CD132 (TUGm2, APC, 1:75, Biolegend, #132307). The same IL2Rα/CD25 antibody was used to assess the expression level of IL2Rα/CD25 in iTreg cells differentiated in the presence of TGFβ + VitC, or endogenous Treg cells from $Tet2^{fl/fl}Tet3^{fl/fl}$ Foxp3-eGFP CD4CRE mice and littermate controls.

Analysis of 5hmC levels using anti-CMS dot blots

Anti-CMS dot blot assay was performed as described previously (Yue *et al*, 2016). Briefly, genomic DNA samples were treated with sodium bisulfite using the Methylcode kit (Invitrogen). Bisulfite-treated DNA samples were then denatured in 0.4 M NaOH, 10 mM EDTA at 95°C for 10 min, and neutralized by adding an equal volume of cold 2 M ammonium acetate (pH 7.0). Twofold serial dilutions of the denatured DNA samples were spotted on a nitrocellulose membrane in an assembled Bio-Dot apparatus (Bio-Rad) according to the manufacturer's instructions. The membrane was washed with 2× SSC buffer, air-dried, and vacuum-baked at 80°C for 2 h, then blocked with 5% non-fat milk for 1hr, and incubated with anti-CMS antibody (1:3,000) overnight at 4°C. After incubating with HRP-conjugated anti-rabbit IgG secondary antibody, the membrane was visualized by enhanced chemiluminescence.

STAT5 phosphorylation

To assess STAT5 phosphorylation, iTreg cells differentiated in the presence of TGFβ alone, TGFβ+ VitC or TGFβ+ RA + VitC were collected and washed on day 6 after differentiation. $1.5–2 \times 10^6$ cells were plated in 100 μl culture medium in a round-bottom 96-well plate. The cells were rested for 1 h at 37°C and then mixed with 100 μl of 2X IL-2 cytokine mix to get a final concentration of 0, 3, 5, 10, and 100 U/ml of IL-2. The cells were then restimulated with IL-2 at 37°C for 1 h. After restimulation, cells were fixed with 4% Paraformaldehyde (Electron Microscopy Sciences) at room temperature for 10 min. The fixed cells were washed twice with MACS buffer, permeabilized by adding 100 μl of ice-cold True-Phos Perm Buffer (BioLegend), and incubated for at least 1 h at −20°C. The cells were then washed twice with MACS buffer, stained with mouse anti-Stat5 (pY694) (Clone: 47/Stat5 (pY694); Alexa Fluor 647; 10 μl/assay; catalog #612599; BD Biosciences) and analyzed by flow cytometry on LSR-II. To examine STAT5 phosphorylation in endogenous Treg cells, $CD4^+$ T cells were isolated from $Tet2^{fl/fl}Tet3^{fl/fl}$ Foxp3-eGFP CD4CRE mice and littermate controls using Dynabeads Untouched Mouse CD4 Cell Kit (Invitrogen) and used for IL-2 restimulation (10 and 100 U/ml

of IL-2). $CD4^+Foxp3^+$ Treg cells were gated to examine the level of STAT5 phosphorylation.

STAT5 ChIP-qPCR

For ChIP assay, iTreg cells differentiated in the presence of TGFβ alone or TGFβ + RA + VitC were collected on day 7 after differentiation and restimulated without or with 3 U/ml IL-2 for 1 h at 37°C. Cells were then fixed with 1% formaldehyde (Thermo Fisher Scientific) at room temperature for 10 min at 1×10^6 cell/ml in culture medium. The reactions were quenched with 125 mM glycine and washed twice with ice-cold 1× PBS. Cells were pelleted, snap-frozen with liquid nitrogen, and stored at −80°C. All the buffers used in the following steps were supplemented with Halt Protease Inhibitor Cocktail (Thermo Fisher Scientific) and phosphatase inhibitor PhosStop (Roche). To isolate nuclei, cell pellets were thawed on ice, resuspended in lysis buffer (50 mM HEPES pH7.5, 140 mM NaCl, 1 mM EDTA, 10% glycerol, 0.5% NP-40, 0.25% Triton X-100), and incubated at 4°C for 10 min with rotation. The cells were then washed twice with washing buffer (10 mM Tris–HCl pH8.0, 200 mM NaCl, 1 mM EDTA and 0.5 mM EGTA), once with shearing buffer (10 mM Tris–HCl pH8.0, 1 mM EDTA, 1% SDS). After the washing steps, nuclei were resuspended in shearing buffer in 1.5ml Bioruptor Pico Microtubes (5×10^6 cells/100 μl) and sonicated using Bioruptor Pico sonication device (Diagenode) for 10 cycles (30 s ON/30 s OFF per cycle). After sonication, chromatin was diluted at a 1:10 ratio with RIPA buffer (10 mM Tris–HCl ph7.5, 140 mM NaCl, 1 mM EDTA, 0.5 mM EGTA, 0.1% SDS, 0.1% sodium deoxycholate, 0.1% Triton X-100) and insoluble debris was removed by centrifugation at 4°C. Protein G magnetic beads were pre-loaded with 5 μg of anti-STAT5A/B antibody (AF2168; R&D Systems) and incubated with the chromatin (pre-cleared with Protein G magnetic beads) overnight at 4°C with rotation. Bead-bound chromatin was washed twice with RIPA buffer, once with high-salt wash buffer (50 mM Tris–HCl pH8.0, 500 mM NaCl, 1 mM EDTA, 1% NP-40 and 0.1% SDS), once with low-salt wash buffer (10 mM Tris–HCl pH8.0, 50 mM NaCl, 1 mM EDTA), and once with TE buffer (10 mM Tris–HCl pH8.0, 1 mM EDTA). Chromatin was eluted from beads with elution buffer (100 mM $NaHCO_3$, 1% SDS) twice for 20 min at room temperature with rotation. 1 mg/ml RNaseA was added and incubated at 37°C for 30min. 0.5 mg/ml Proteinase K (Ambion) was then added. The chromatin was de-crosslinked at 65°C overnight with constant shaking. DNA was then purified with ChIP DNA Clean & Concentrator (Zymo Research). Quantitative real-time PCR was performed using FastStart Universal SYBR Green Master mix (Roche) on a StepOnePlus real-time PCR machine (Thermo Fisher Scientific). Primers used for Foxp3 CNS2 and Gmpr are from reference (Zheng *et al*, 2010). Primers used for Il2ra IN1b are as following and are designed based on the reference (Li *et al*, 2017).

Il2ra IN1b forward primer: CCA TTT GAA ACA AGC CCT CAC G
Il2ra IN1b reverse primer: GGG CCA TAT TTT TAG CGG AGC

Data availability

The authors declare that all data supporting the findings of this study are available within the article and its Appendix information files or from the corresponding author upon reasonable request. All code is available upon request. RNA-seq, ATAC-seq, CMS-IP, and WGBS data are deposited in the Gene Expression Omnibus database with the accession number GSE141152 and can be accessed with the link: https://www.ncbi.nlm.nih.gov/geo/query/acc.cgi?acc=GSE141152

Expanded View for this article is available online.

Acknowledgements
We thank Dr. C-W. J. Lio for critical reading of the manuscript and other members of the Rao laboratory for suggestions and discussions. We thank C. Kim, D. Hinz, L. Boggeman, C. Dillingham, and M. Haynes at the La Jolla Institute Flow Cytometry facility for help with cell sorting experiments; and J. Day of the La Jolla Institute Sequencing facility for help with next-generation sequencing. This work was supported by National Institutes of Health (NIH) R01 grants R35 CA210043 and AI 12858901 (to A.R.). The FACSAria II Cell Sorter was acquired through the Shared Instrumentation Grant (SIG) Program S10 RR027366 and the Hiseq 2500 was funded by S10OD016262. D.S.C. and E.G.A are supported by the CONACYT/UCMEXUS fellowship. X.L. was supported by a postdoctoral Fellowship from CIRM UCSD Interdisciplinary Stem Cell Research & Training Grant II (TG2-01154). B.G.B is supported by institutional funds, a postdoctoral Fellowship from the American Cancer Society (PF-17-109-1-TBG), a Multiple Myeloma Research Foundation Fellowship, and an American Society of Hematology Scholar Award.

Author contributions
Project conception: AR and XY; Experiments and analysis and interpretation of results: XY and XL; Bioinformatics and statistical analyses (RNA-seq, CMS-IP, WGBS, and ATAC-seq): DS-C and BGB; Initial analysis for CMS-IP and WGBS data: EG-A; Supervision of the bioinformatics analyses: BGB; Input for the biological aspects of the bioinformatics analyses: AR and XY; Supervision of project planning and execution: AR; Manuscript writing: AR, XY, and BGB; Proofreading the manuscript and editorial input: all authors.

Conflict of interest
A.R. is a member of the Scientific Advisory Board of Cambridge EpiGenetix, Ltd., Cambridge, UK. None of the other authors has any competing interests.

References

Abbas AK, Trotta E, Simeonov D, Marson A, Bluestone JA (2018) Revisiting IL-2: biology and therapeutic prospects. *Sci Immunol* 3: eaat1482

Barwick BG, Scharer CD, Bally APR, Boss JM (2016) Plasma cell differentiation is coupled to division-dependent DNA hypomethylation and gene regulation. *Nat Immunol* 17: 1216–1225

Barwick BG, Scharer CD, Martinez RJ, Price MJ, Wein AN, Haines RR, Bally APR, Kohlmeier JE, Boss JM (2018) B cell activation and plasma cell differentiation are inhibited by de novo DNA methylation. *Nat Commun* 9: 1900

Blaschke K, Ebata KT, Karimi MM, Zepeda-Martinez JA, Goyal P, Mahapatra S, Tam A, Laird DJ, Hirst M, Rao A *et al* (2013) Vitamin C induces Tet-dependent DNA demethylation and a blastocyst-like state in ES cells. *Nature* 500: 222–226

Buenrostro JD, Giresi PG, Zaba LC, Chang HY, Greenleaf WJ (2013) Transposition of native chromatin for fast and sensitive epigenomic profiling of open chromatin, DNA-binding proteins and nucleosome position. *Nat Methods* 10: 1213–1218

Chinen T, Kannan AK, Levine AG, Fan X, Klein U, Zheng Y, Gasteiger G, Feng Y, Fontenot JD, Rudensky AY (2016) An essential role for the IL-2 receptor in Treg cell function. *Nat Immunol* 17: 1322–1333

Dang L, Su SM (2017) Isocitrate dehydrogenase mutation and (R)-2-hydroxyglutarate: from basic discovery to therapeutics development. *Annu Rev Biochem* 86: 305–331

Dobin A, Davis CA, Schlesinger F, Drenkow J, Zaleski C, Jha S, Batut P, Chaisson M, Gingeras TR (2013) STAR: ultrafast universal RNA-seq aligner. *Bioinformatics* 29: 15–21

Feng H, Conneely KN, Wu H (2014a) A Bayesian hierarchical model to detect differentially methylated loci from single nucleotide resolution sequencing data. *Nucleic Acids Res* 42: e69

Feng Y, Arvey A, Chinen T, van der Veeken J, Gasteiger G, Rudensky AY (2014b) Control of the inheritance of regulatory T cell identity by a cis element in the Foxp3 locus. *Cell* 158: 749–763

Floess S, Freyer J, Siewert C, Baron U, Olek S, Polansky J, Schlawe K, Chang H-D, Bopp T, Schmitt E *et al* (2007) Epigenetic control of the foxp3 locus in regulatory T cells. *PLoS Biol* 5: e38

Fontenot JD, Rasmussen JP, Gavin MA, Rudensky AY (2005) A function for interleukin 2 in Foxp3-expressing regulatory T cells. *Nat Immunol* 6: 1142–1151

Gentleman RC, Carey VJ, Bates DM, Bolstad B, Dettling M, Dudoit S, Ellis B, Gautier L, Ge Y, Gentry J *et al* (2004) Bioconductor: open software development for computational biology and bioinformatics. *Genome Biol* 5: R80

Grinberg-Bleyer Y, Oh H, Desrichard A, Bhatt DM, Caron R, Chan TA, Schmid RM, Klein U, Hayden MS, Ghosh S (2017) NF-κB c-Rel is crucial for the regulatory T cell immune checkpoint in cancer. *Cell* 170: 1096–1108.e13

Hausinger RP (2004) FeII/alpha-ketoglutarate-dependent hydroxylases and related enzymes. *Crit Rev Biochem Mol Biol* 39: 21–68

Hayatsu N, Miyao T, Tachibana M, Murakami R, Kimura A, Kato T, Kawakami E, Endo TA, Setoguchi R, Watarai H *et al* (2017) Analyses of a mutant Foxp3 allele reveal BATF as a critical transcription factor in the differentiation and accumulation of tissue regulatory T cells. *Immunity* 47: 268–283.e9

He Y-F, Li B-Z, Li Z, Liu P, Wang Y, Tang Q, Ding J, Jia Y, Chen Z, Li L *et al* (2011) Tet-mediated formation of 5-carboxylcytosine and its excision by TDG in mammalian DNA. *Science* 333: 1303–1307

Heinz S, Benner C, Spann N, Bertolino E, Lin YC, Laslo P, Cheng JX, Murre C, Singh H, Glass CK (2010) Simple combinations of lineage-determining transcription factors prime cis-regulatory elements required for macrophage and B cell identities. *Mol Cell* 38: 576–589

Hill JA, Feuerer M, Tash K, Haxhinasto S, Perez J, Melamed R, Mathis D, Benoist C (2007) Foxp3 transcription-factor-dependent and -independent regulation of the regulatory T cell transcriptional signature. *Immunity* 27: 786–800

Huang Y, Pastor WA, Shen Y, Tahiliani M, Liu DR, Rao A (2010) The behaviour of 5-hydroxymethylcytosine in bisulfite sequencing. *PLoS One* 5: e8888

Huang Y, Pastor WA, Zepeda-Martinez JA, Rao A (2012) The anti-CMS technique for genome-wide mapping of 5-hydroxymethylcytosine. *Nat Protoc* 7: 1897–1908

Huehn J, Polansky JK, Hamann A (2009) Epigenetic control of FOXP3 expression: the key to a stable regulatory T-cell lineage? *Nat Rev Immunol* 9: 83–89

Huijskens MJ, Wodzig WK, Walczak M, Germeraad WT, Bos GM (2016) Ascorbic acid serum levels are reduced in patients with hematological malignancies. *Results Immunol* 6: 8–10

Ito S, Shen L, Dai Q, Wu SC, Collins LB, Swenberg JA, He C, Zhang Y (2011) Tet proteins can convert 5-methylcytosine to 5-formylcytosine and 5-carboxylcytosine. *Science* 333: 1300–1303

Iyer LM, Tahiliani M, Rao A, Aravind L (2009) Prediction of novel families of enzymes involved in oxidative and other complex modifications of bases in nucleic acids. *Cell Cycle* 8: 1698–1710

Josefowicz SZ, Lu LF, Rudensky AY (2012) Regulatory T cells: mechanisms of differentiation and function. *Annu Rev Immunol* 30: 531–564

Khaw KT, Bingham S, Welch A, Luben R, Wareham N, Oakes S, Day N (2001) Relation between plasma ascorbic acid and mortality in men and women in EPIC-Norfolk prospective study: a prospective population study. European Prospective Investigation into Cancer and Nutrition. *Lancet* 357: 657–663

Koizumi S-I, Sasaki D, Hsieh T-H, Taira N, Arakaki N, Yamasaki S, Wang Ke, Sarkar S, Shirahata H, Miyagi M *et al* (2018) JunB regulates homeostasis and suppressive functions of effector regulatory T cells. *Nat Commun* 9: 5344

Krueger F, Andrews SR (2011) Bismark: a flexible aligner and methylation caller for Bisulfite-Seq applications. *Bioinformatics* 27: 1571–1572

Langmead B, Salzberg SL (2012) Fast gapped-read alignment with Bowtie 2. *Nat Methods* 9: 357–359

Laurent L, Wong E, Li G, Huynh T, Tsirigos A, Ong CT, Low HM, Kin Sung KW, Rigoutsos I, Loring J *et al* (2010) Dynamic changes in the human methylome during differentiation. *Genome Res* 20: 320–331

Lawrence M, Gentleman R, Carey V (2009) rtracklayer: an R package for interfacing with genome browsers. *Bioinformatics* 25: 1841–1842

Lawrence M, Huber W, Pages H, Aboyoun P, Carlson M, Gentleman R, Morgan MT, Carey VJ (2013) Software for computing and annotating genomic ranges. *PLoS Comput Biol* 9: e1003118

Lee DU, Agarwal S, Rao A (2002) Th2 lineage commitment and efficient IL-4 production involves extended demethylation of the IL-4 gene. *Immunity* 16: 649–660

Li H, Handsaker B, Wysoker A, Fennell T, Ruan J, Homer N, Marth G, Abecasis G, Durbin R, Genome Project Data Processing S (2009) The sequence Alignment/Map format and SAMtools. *Bioinformatics* 25: 2078–2079

Li P, Mitra S, Spolski R, Oh J, Liao W, Tang Z, Mo F, Li X, West EE, Gromer D *et al* (2017) STAT5-mediated chromatin interactions in superenhancers activate IL-2 highly inducible genes: functional dissection of the Il2ra gene locus. *Proc Natl Acad Sci USA* 114: 12111–12119

Li X, Liang Y, LeBlanc M, Benner C, Zheng Y (2014) Function of a Foxp3 cis-element in protecting regulatory T cell identity. *Cell* 158: 734–748

Li X, Zheng Y (2015) Regulatory T cell identity: formation and maintenance. *Trends Immunol* 36: 344–353

Liberzon A, Birger C, Thorvaldsdóttir H, Ghandi M, Mesirov JP, Tamayo P (2015) The molecular signatures database (MSigDB) hallmark gene set collection. *Cell Syst* 1: 417–425

Lio CJ, Rao A (2019) TET enzymes and 5hmC in adaptive and innate immune systems. *Front Immunol* 10: 210

Lio CJ, Shukla V, Samaniego-Castruita D, Gonzalez-Avalos E, Chakraborty A, Yue X, Schatz DG, Ay F, Rao A (2019a) TET enzymes augment activation-induced deaminase (AID) expression via 5-hydroxymethylcytosine modifications at the *Aicda superenhancer*. *Sci Immunol* 4: eaau7523

Lio CJ, Yue X, Lopez-Moyado IF, Tahiliani M, Aravind L, Rao A (2020) TET methylcytosine oxidases: new insights from a decade of research. *J Biosci* 45: 21

Lio CJ, Yuita H, Rao A (2019b) Dysregulation of the TET family of epigenetic regulators in lymphoid and myeloid malignancies. *Blood* 134: 1487–1497

Lio CW, Zhang J, González-Avalos E, Hogan PG, Chang X, Rao A (2016) Tet2 and Tet3 cooperate with B-lineage transcription factors to regulate DNA modification and chromatin accessibility. *Elife* 5: e18290

Lopez-Moyado IF, Tsagaratou A, Yuita H, Seo H, Delatte B, Heinz S, Benner C, Rao A (2019) Paradoxical association of TET loss of function with genome-wide DNA hypomethylation. *Proc Natl Acad Sci USA* 116: 16933–16942

Loria CM, Klag MJ, Caulfield LE, Whelton PK (2000) Vitamin C status and mortality in US adults. *Am J Clin Nutr* 72: 139–145

Luo CT, Osmanbeyoglu HU, Do MH, Bivona MR, Toure A, Kang D, Xie Y, Leslie CS, Li MO (2017) Ets transcription factor GABP controls T cell homeostasis and immunity. *Nat Commun* 8: 1062

McLean CY, Bristor D, Hiller M, Clarke SL, Schaar BT, Lowe CB, Wenger AM, Bejerano G (2010) GREAT improves functional interpretation of cis-regulatory regions. *Nat Biotechnol* 28: 495–501

Mouly E, Chemin K, Nguyen HV, Chopin M, Mesnard L, Leite-de-Moraes M, Burlen-defranoux O, Bandeira A, Bories JC (2010) The Ets-1 transcription factor controls the development and function of natural regulatory T cells. *J Exp Med* 207: 2113–2125

Muthusamy N, Barton K, Leiden JM (1995) Defective activation and survival of T cells lacking the Ets-1 transcription factor. *Nature* 377: 639–642

Neri F, Incarnato D, Krepelova A, Rapelli S, Pagnani A, Zecchina R, Parlato C, Oliviero S (2013) Genome-wide analysis identifies a functional association of Tet1 and Polycomb repressive complex 2 in mouse embryonic stem cells. *Genome Biol* 14: R91

Pastor WA, Aravind L, Rao A (2013) TETonic shift: Biological roles of TET proteins in DNA demethylation and transcription. *Nat Rev Mol Cell Biol* 14: 341–356

Pastor WA, Pape UJ, Huang Y, Henderson HR, Lister R, Ko M, McLoughlin EM, Brudno Y, Mahapatra S, Kapranov P *et al* (2011) Genome-wide mapping of 5-hydroxymethylcytosine in embryonic stem cells. *Nature* 473: 394–397

Robinson MD, McCarthy DJ, Smyth GK (2010) edgeR: a Bioconductor package for differential expression analysis of digital gene expression data. *Bioinformatics* 26: 139–140

Ronin E, Lubrano di Ricco M, Vallion R, Divoux J, Kwon H-K, Grégoire S, Collares D, Rouers A, Baud V, Benoist C *et al* (2019) The NF-κB RelA transcription factor is critical for regulatory T cell activation and stability. *Front Immunol* 10: 2487

Ross SH, Cantrell DA (2018) Signaling and function of interleukin-2 in T lymphocytes. *Annu Rev Immunol* 36: 411–433

Roychoudhuri R, Hirahara K, Mousavi K, Clever D, Klebanoff CA, Bonelli M, Sciumè G, Zare H, Vahedi G, Dema B *et al* (2013) BACH2 represses effector programs to stabilize T(reg)-mediated immune homeostasis. *Nature* 498: 506–510

Sakaguchi S, Yamaguchi T, Nomura T, Ono M (2008) Regulatory T cells and immune tolerance. *Cell* 133: 775–787

Samstein R, Arvey A, Josefowicz S, Peng X, Reynolds A, Sandstrom R, Neph S, Sabo P, Kim J, Liao W *et al* (2012) Foxp3 exploits a pre-existent enhancer landscape for regulatory T cell lineage specification. *Cell* 151: 153–166

Sardina JL, Collombet S, Tian TV, Gómez A, Di Stefano B, Berenguer C, Brumbaugh J, Stadhouders R, Segura-Morales C, Gut M *et al* (2018) Transcription factors drive Tet2-mediated enhancer demethylation to reprogram cell fate. *Cell Stem Cell* 23: 727–741 e729

Sasidharan Nair V, Song MH, Oh KI (2016) Vitamin C facilitates demethylation of the Foxp3 enhancer in a tet-dependent manner. *J Immunol* 196: 2119–2131

Sekiya T, Kashiwagi I, Yoshida R, Fukaya T, Morita R, Kimura A, Ichinose H, Metzger D, Chambon P, Yoshimura A (2013) Nr4a receptors are essential for thymic regulatory T cell development and immune homeostasis. *Nat Immunol* 14: 230–237

Snow JW, Abraham N, Ma MC, Herndier BG, Pastuszak AW, Goldsmith MA (2003) Loss of tolerance and autoimmunity affecting multiple organs in STAT5A/5B-deficient mice. *J Immunol* 171: 5042–5050

Subramanian A, Tamayo P, Mootha Vk, Mukherjee S, Ebert Bl, Gillette Ma, Paulovich A, Pomeroy Sl, Golub Tr, Lander Es *et al* (2005) Gene set enrichment analysis: a knowledge-based approach for interpreting genome-wide expression profiles. *Proc Natl Acad Sci USA* 102: 15545–15550

Suzuki T, Shimizu Y, Furuhata E, Maeda S, Kishima M, Nishimura H, Enomoto S, Hayashizaki Y, Suzuki H (2017) RUNX1 regulates site specificity of DNA demethylation by recruitment of DNA demethylation machineries in hematopoietic cells. *Blood Adv* 1: 1699–1711

Tahiliani M, Koh KP, Shen Y, Pastor WA, Bandukwala H, Brudno Y, Agarwal S, Iyer LM, Liu DR, Aravind L *et al* (2009) Conversion of 5-methylcytosine to 5-hydroxymethylcytosine in mammalian DNA by MLL partner TET1. *Science* 324: 930–935

Toker A, Huehn J (2011) To be or not to be a Treg cell: lineage decisions controlled by epigenetic mechanisms. *Sci Signal* 4: pe4

Toomer KH, Lui JB, Altman NH, Ban Y, Chen X, Malek TR (2019) Essential and non-overlapping IL-2Ralpha-dependent processes for thymic development and peripheral homeostasis of regulatory T cells. *Nat Commun* 10: 1037

Tsagaratou A, Aijo T, Lio CW, Yue X, Huang Y, Jacobsen SE, Lahdesmaki H, Rao A (2014) Dissecting the dynamic changes of 5-hydroxymethylcytosine in T-cell development and differentiation. *Proc Natl Acad Sci USA* 111: E3306–3315

Tsagaratou A, González-Avalos E, Rautio S, Scott-Browne JP, Togher S, Pastor WA, Rothenberg EV, Chavez L, Lähdesmäki H, Rao A (2017a) TET proteins regulate the lineage specification and TCR-mediated expansion of iNKT cells. *Nat Immunol* 18: 45–53

Tsagaratou A, Lio CJ, Yue X, Rao A (2017b) TET Methylcytosine oxidases in T cell and B cell development and function. *Front Immunol* 8: 220

Tsagaratou A, Rao A (2013) TET proteins and 5-methylcytosine oxidation in the immune system. *Cold Spring Harb Symp Quant Biol* 78: 1–10

Wang Y, Xiao M, Chen X, Chen L, Xu Y, Lv L, Wang Pu, Yang H, Ma S, Lin H *et al* (2015) WT1 recruits TET2 to regulate its target gene expression and suppress leukemia cell proliferation. *Mol Cell* 57: 662–673

Wu X, Zhang Y (2017) TET-mediated active DNA demethylation: mechanism, function and beyond. *Nat Rev Genet* 18: 517–534

Wu Y, Borde M, Heissmeyer V, Feuerer M, Lapan AD, Stroud JC, Bates DL, Guo L, Han A, Ziegler SF *et al* (2006) FOXP3 controls regulatory T cell function through cooperation with NFAT. *Cell* 126: 375–387

Xu W, Yang H, Liu Y, Yang Y, Wang P, Kim SH, Ito S, Yang C, Wang P, Xiao MT *et al* (2011) Oncometabolite 2-hydroxyglutarate is a competitive inhibitor of alpha-ketoglutarate-dependent dioxygenases. *Cancer Cell* 19: 17–30

Yang R, Qu C, Zhou Yu, Konkel JE, Shi S, Liu Yi, Chen C, Liu S, Liu D, Chen Y *et al* (2015) Hydrogen sulfide promotes Tet1- and Tet2-Mediated Foxp3 demethylation to drive regulatory T cell differentiation and maintain immune homeostasis. *Immunity* 43: 251–263

Ye D, Guan KL, Xiong Y (2018) Metabolism, activity, and targeting of D- and L-2-hydroxyglutarates. *Trends Cancer* 4: 151–165

Yoshida H, Lareau CA, Ramirez RN, Rose SA, Maier B, Wroblewska A, Desland F, Chudnovskiy A, Mortha A, Dominguez C *et al* (2019) The cis-regulatory atlas of the mouse immune system. *Cell* 176: 897–912.e20

Yue X, Lio CJ, Samaniego-Castruita D, Li X, Rao A (2019) Loss of TET2 and TET3 in regulatory T cells unleashes effector function. *Nat Commun* 10: 2011

Yue X, Rao A (2020) TET-family dioxygenases and the TET activator Vitamin C in immune responses and cancer. *Blood* 136: 1394–1401

Yue X, Trifari S, Äijö T, Tsagaratou A, Pastor WA, Zepeda-Martínez JA, Lio C-W, Li X, Huang Y, Vijayanand P *et al* (2016) Control of Foxp3 stability through modulation of TET activity. *J Exp Med* 213: 377–397

Zhang Y, Liu T, Meyer CA, Eeckhoute J, Johnson DS, Bernstein BE, Nussbaum C, Myers RM, Brown M, Li W *et al* (2008) Model-based analysis of ChIP-Seq (MACS). *Genome Biol* 9: R137

Zheng Y, Josefowicz S, Chaudhry A, Peng XP, Forbush K, Rudensky AY (2010) Role of conserved non-coding DNA elements in the Foxp3 gene in regulatory T-cell fate. *Nature* 463: 808–812